Ground-based observation of clusters and nucleation mode particles in the Amazon

Daniela Wimmer[1], Stephany Buenrostro Mazon[1], Hanna Elina Manninen[1,2], Juha Kangasluoma[1], Alessandro Franchin[1,3,4], Tuomo Nieminen[1,5], John Backman[6], Jian Wang[8], Chongai Kuang[8], Radovan Krejci[7], Joel Brito[9,10], Fernando Goncalves Morais[9], Scot Turnbull Martin[11], Paulo Artaxo[9], Markku Kulmala[1], Veli-Matti Kerminen[1] and Tuukka Petäjä[1]

[1]Department of Physics, University of Helsinki, Gustaf Hallströmin katu 2a, 00560, Helsinki, Finland
[2]European Organization for Nuclear Research (CERN), 1211 Geneva, Switzerland
[3]NOAA Earth System Research Laboratory (ESRL), Chemical Sciences Division, Boulder, CO, USA
[4]Cooperative Institute for Research in Environmental Sciences, University of Colorado Boulder, Boulder, CO, USA
[5]Department of Applied Physics, University of Eastern Finland, Post Office Box 1627, 70211 Kuopio, Finland
[6]Finnish Meteorological Institute, Atmospheric composition research, Erik Palménin aukio 1, 00560, Helsinki, Finland
[7]Stockholm University, Department of Environmental Science and Analytical Chemistry (ACES), 106 91 Stockholm, Sweden
[8]Environmental and Climate Sciences Department, Brookhaven National Laboratory, Upton, New York, USA
[9]Institute of Physics, University of São Paulo, de Fisica, Universidade de Sao Paulo, Rua do Matao 1371, CEP 05508-090, Sao Paulo, Brazil
[10]Laboratory for Meteorological Physics (LaMP), Université Clermont Auvergne, F-63000 Clermont-Ferrand, France
[11]School of Engineering and Applied Sciences, Harvard University Cambridge, Massachusetts 02138, United States of America

Correspondence to: Daniela Wimmer (daniela.wimmer@helsinki.fi)
Keywords: atmospheric ions, particle formation, rainforest, high-frequency rainfall

Abstract

We investigated atmospheric new particle formation (NPF) in the Amazon rainforest using direct measurement methods. To our knowledge this is the first direct observation of NPF events in the Amazon region. However, previous observations elsewhere in Brazil showed the occurrence of nucleation mode particles. Our measurements covered two field sites and both wet and dry season. We measured the variability of air ion concentrations (0.8 – 12 nm) with an ion spectrometer

between September 2011 and January 2014 at a rainforest site (T0t). Between February and October 2014, the same measurements were performed at a grassland pasture site (T3) as part of the GoAmazon 2014/5 Experiment, with two intensive operating periods (IOP1 and IOP2 during the wet and the dry season respectively). The GoAmazon 2014/5 Experiment was designed to study the influence of anthropogenic emissions on the changing climate in the Amazon region. The experiment included basic aerosol and trace gas measurements at the ground, remote sensing instrumentation and two aircraft-based measurements.

The results presented in this work are from measurements performed at ground level at both sites. The site inside the rainforest (T0t) is located 60 km NNW of Manaus and influenced by pollution about once per week. The pasture (T3) site is located 70 km downwind from Manaus and influenced by the Manaus pollution plume typically once per day or every second day, especially in the afternoon. No new particle formation (NPF) events were observed inside the rainforest (site T0t) at ground level during the measurement period. However, rain-induced ion and particle bursts (hereafter, "rain-events") occurred frequently (643/1031 days) at both sites during the wet and dry season, being most frequently during the wet season. During the rain-events, the ion concentrations in three size ranges (0.8-2 nm, 2-4 nm and 4-12 nm) increased up to about 10^4 - 10^5 cm^{-3}. This effect was most pronounced in the intermediate and large size ranges, where the background ion concentrations were about 10 – 15 cm^{-3}, as compared with 700 cm^{-3} for the cluster ion background. We observed 8 NPF events at the pasture site during the wet season. We calculated the growth rates and formation rates of neutral particles and ions for the size ranges 2-3 nm and 3-7 nm using the ion spectrometer data. The observed median growth rates were 0.8 nm h^{-1} and 1.6 nm h^{-1} for 2-3 nm-sized ions and particles, respectively, with larger growth rates (13.3 nm h^{-1} and 7.9 nm h^{-1}) in the 3-7 nm size range. The measured nucleation rates were of the order of 0.2 cm^{-3} s^{-1} for particles and 4-9x10^{-3} cm^{-3} s^{-1} for ions. There was no clear difference in the sulfuric acid concentrations between the NPF event days and non-event days (~9x10^5 cm^{-3}). The two major differences between the NPF days and non-event days were a factor of 1.8 lower condensation sink on NPF event days (1.8x10^{-3} s^{-1}) compared to non-events (3.2x10^{-3} s^{-1}) and different air mass origins.

To our knowledge, this is the first time that results from ground-based sub-3 nm aerosol particle measurements have been obtained from the Amazon rainforest.

1 Introduction

Globally, atmospheric new particle formation (NPF) and growth has been estimated to account for a major, if not dominant, fraction of cloud condensation nuclei (Merikanto et al. 2009, Wang and Penner, 2009, Yu and Luo, 2009, Dunne et al., 2016, Kulmala et al., 2016). The formation of atmospheric nanoparticles is a multi-stage process, in which stable clusters form from gas phase precursors, followed by the activation of these clusters and their further growth (Kulmala et al. 2014). Although atmospheric NPF is occurring frequently in many environments (e.g. Kulmala et al. 2004, Manninen et al. 2010), the Amazon basin is one of the locations where the initial steps of the formation of nanoparticles have not been previously observed from ground-based measurements (Martin et al, 2010a).

In the Amazon basin, emissions and oxidation of volatile organic compounds (e.g. Lelieveld et al. 2008), aerosol activation to cloud droplets, and eventually rain formation, are tightly connected with synoptic processes, such as deep convection (e.g. Lelieveld et al. 2008, Wang et al., 2016). Aerosol concentrations in the Amazonian atmosphere are rapidly changing as a result of deforestation and the associated biomass burning and economic development in the Amazon region (Martin et al. 2016, Artaxo et al., 2013). The Manaus metropolis (population 2 million) is the capital of the state of Amazonia, Brazil, surrounded by the largest rainforest on Earth (Martin et al, 2017), as shown in Fig. 1.

The measurements discussed in this paper took place at two different locations in the Amazon rainforest: a pasture site 70 km downwind from Manaus (T3; Martin et al., 2016); and a site within the rainforest, mostly unaffected by Manaus pollution (T0t; Martin et al., 2010b). The sites are described in more detail in section 2.1. Depending on the wind direction, these sites can represent (i) one of the most anthropogenically undisturbed continental locations on Earth, or (ii) a location affected by both polluted and clean air masses (Martin et al., 2016). The complexity of the mixture of trace gases and aerosol population make the Amazon rainforest an interesting place to study. During most of the wet season, the Amazon basin is one of the cleanest continental regions on Earth (Andreae, 2007; Martin et al., 2010a, Artaxo et al., 2013, Andreae et al., 2015). During the dry season, the Amazon basin is highly influenced by anthropogenic emissions mostly from biomass burning. Additionally, our study region experiences frequent high-intensity precipitation episodes.

The primary goal of this paper was to investigate the characteristics of the wet and the dry season at different sampling locations and the occurrence of new particle formation (NPF) and growth in the Amazon region, and to quantify the role of ions and aerosol particles in this process.

2 Methods

The measurements inside the rainforest at site T0t were performed over 3 years from September 2011 to January 2014. The second measurement site (T3) was part of the Green Ocean Amazon (GoAmazon2014/5) Experiment (Martin et al., 2016). The GoAmazon2014/5 Experiment operated from January 1, 2014 to December 31, 2015. The experiment included two intensive operation periods (IOP1 and IOP2). IOP1 extended from February 1, 2014 to March 31, 2014 and IOP2 from August 15, 2014 to October 15, 2014 (Martin et al., 2016). The ion spectrometer measurements were conducted from January 28 to October 13, 2014. Figure 1 shows the locations of both measurement sites. Table 1 shows an overview over the available dataset presented in this study.

2.1. Measurement sites

2.1.1 Measurement site inside the rainforest

The T0t ecological reserve (Martin et al, 2010b) is a terrestrial ecosystem science measurement site located 70 km NNW of the Manaus metropolis in the central region of Brazil (2.609°S, 60.2092°W).

Two major rivers, the Solimoes and the Rio Negro converge in Manaus to become the Amazon river. The city of Manaus is the capital of the state of Amazonia, Brazil, with more than 2 million inhabitants (IBGE, 2015). It is the seventh biggest city in Brazil and is surrounded by forest for 1500 km in all directions (Martin et al., 2016).

T0t is surrounded by a dense rainforest. The rainforest canopy is homogeneous with an average height of 30 m. T0t is influenced by anthropogenic pollution about once per week (Martin et al., 2010b supplementary material, Thalmann et al, 2017, de Sa et al, 2017). Otherwise, the location of the T0t site allows the characterization of an almost completely undisturbed environment (Martin et al, 2016).

2.1.2 Open pasture measurement site

The open pasture site, T3, is influenced by the Manaus pollution plume typically once per day or every second day, especially in the afternoon (Martin et al., 2010b supplementary material, Thalmann et al, 2017, de Sa et al, 2017). A Mobile Facility from the Atmospheric Radiation Measurement (ARM) Program (Mather et al., 2014) of the United States Department of Energy was deployed at the T3 site close to Manacapuru, about 70 km downwind of the city of Manaus (3.2133°S, 60.5987°W), and included an ARM Mobile Aerosol Observing System (MAOS). The site also hosted numerous instrument systems from other GoAmazon2014/5 participants (Martin et al., 2016).

2.2 Instrumentation

2.2.1 Neutral cluster and Air Ion Spectrometer (NAIS)

A Neutral cluster and Air Ion Spectrometer (NAIS; Manninen et al., 2016) was used to determine the early stages of atmospheric nucleation and subsequent growth. The NAIS measures the mobility distributions in the range 3.2 – 0.0013 $cm^2\ V^{-1}\ s^{-1}$, which corresponds to a mobility equivalent diameter range of 0.8 – 42 nm. The ion and neutral particle size distributions are measured in three different stages: ion, particle, and offset. The NAIS consists of two parallel cylindrical DMAs (Differential Mobility Analyzers), one for classifying negative ions and the other for positive ions. In the ion mode, the corona chargers and the electrostatic filters are switched off to allow only naturally-charged ions to enter the DMA. During the particle mode, the particles are charged by a corona charger in order to be detected by the DMA. The inlet flow into the NAIS is 60 liters per minute (Lpm), whereas the sample and the sheath flows of the DMAs are 30 and 60 Lpm, respectively. The NAIS time resolution was set to 5 min, which includes a full measurement cycle of negative ions, positive ions and total particles. The NAIS instrument and calibration are described in more details in Asmi et al. (2009), Wagner et al. (2016) and Manninen et al. (2016). The NAIS measurement accuracy was estimated to be 10 - 30%, which was mainly due to flow rate uncertainties (Manninen et al., 2016; Wagner et al., 2016). The electrometers measure a current

which can be transformed into particle/ion concentrations. If the measured currents are low, the noise can be quite high and can result in negative concentration values. The environmental conditions in the Amazon are very challenging for NAIS measurements, especially the high relative humidity (RH). To reduce the NAIS sampling RH, an electric heater was installed at the inlet to heat the sampling air to 60° C in order to evaporate some water before entering the instrument.

The NAIS was placed inside a hut at the T0t site, sampling at 2 m above the ground level. In January 2014, the NAIS was moved to the T3 site where it was placed outside under a roof. The sampling setup was the same at both sites. In total 736 days of neutral particle data and 718 days of ion data were taken at both sites together (see Table 1).

2.2.2 Particle Size Magnifier (PSM)

A Particle Size Magnifier (PSM; Airmodus A09; Vanhanen et al., 2011) was used to determine aerosol particle concentrations at sizes below 3 nm. The PSM is a mixing-type condensation particle counter (CPC), in which the aerosol is turbulently mixed with air saturated with diethylene glycol (DEG). DEG only grows the particles to about 90 nm, so the PSM system consists of a second stage, where the particles are grown to optically-detectable sizes. The 50% activation diameter of the instrument can be varied across a size range of 1–4 nm in a mobility diameter (Vanhanen et al., 2011) by changing the mixing ratio between the saturator and the sample flow. At GoAmazon2014/5, the PSM was used in a scanning mode in which the saturator flow is continuously changing, altering the cut-off diameters between 1 and 4 nm. One scan takes 4 minutes and the system was set up to do one upscan, followed by a downscan. Due to the challenging measurement conditions, the size-resolved data was not used in this analysis.

Prior to the deployment during the GoAmazon2014/5 campaign, the PSM system was equipped with an inlet system specifically designed to decrease the relative humidity of the sample without disturbing the sample itself and to maintain high flow rates to minimize diffusion losses. The inlet system comprises a core sampling probe combined with a sintered tube. The core sampling probe consists of two cylindrical tubes with different outer diameters (10 mm and 6 mm). The larger diameter of the outer tube allows a total laminar flow rate of up to 10 Lpm, to minimize diffusional losses. The inner tube is directly attached to the PSM with an airflow of 2.5 Lpm. The excess airflow is discarded into an exhaust line (Kangasluoma et al., 2016). Downstream of the core sampling line there is a sintered tube where dry, pressurized air is introduced. The water molecules in the sample flow are pushed towards the outer walls of the sintered material by diffusion, drying the airflow. Laboratory studies have shown that RH can drastically affect the PSM counting efficiency (higher sensitivity at smaller sizes at higher RH; Kangasluoma et al, 2013, Iida et al, 2009).

Since the aerosol in Brazil was expected to be composed of mostly organic species, the PSM with the inlet was calibrated using limonene and its oxidation products (Kangasluoma et al., 2014) as a test aerosol. The resulting lowest PSM cut-off diameter was 1.5 nm (±0.3 nm), where the uncertainty

was estimated as a combination of the calibration uncertainty and the influence of the ambient RH on the PSM cut-off diameter. In total, 38 days of data obtained during the dry season were used.

2.2.3. Supporting instrumentation at both sites

At T0t, the submicron aerosol number size distributions and total particle number concentrations were monitored with a DMPS system (Aalto et al., 2001) and a CPC. The CPC time resolution was 1 minute, with a 50% cut-off size of about 6 nm. The DMPS measured number size distributions over the mobility diameter range of 6 – 800 nm (Backman et al., 2012), and a complete size distribution was obtained every 10 minutes. During the 10-minute measurement cycle, size-segregated aerosols were measured for 8 minutes, followed by 2 minutes of total particle number concentration measurements, using a bypass valve. The transmission at 4 nm of the inlet used the AMAZE-08 (Martin et al., 2010b) experiment was 50%. The diffusion losses increase exponentially with a decreasing particle size. For the measurements reported here, a similar setup with a 60 m sampling line was used. The DMPS data should be used in a qualitative rather than quantitative manner as the losses due to diffusion in the sampling line are not precisely known and therefore not considered. In addition to the ion spectrometer measurements, the measurement hut hosted an automated weather system (Vaisala; WXT-520) for acquiring meteorological parameters.

The auxiliary data from the T3 site, presented in this manuscript includes measurements from an ultrafine CPC (TSI Inc; 3010), with a 50% activation diameter of 10 nm and an SMPS with a lower cut-off of 20 nm. The meteorological data were also retrieved from an automated weather station (Vaisala; WXT-520). Those datasets are available at the ARM data browser.

2.3 Measurement periods: wet and dry season

The differences in the tropical seasons present contrasting environmental conditions (Martin et al., 2016, Artaxo et al., 2013). In our manuscript, we follow Artaxo et al. (2013) and define the wet season in the Amazon from January to June, and the dry season from July to December.

The most dominant anthropogenic influence in the Amazon region is dictated by biomass burning emissions, which are strongest during the dry season. The most intense biomass burning and atmospheric perturbations take place at the southern and eastern edges of the forest (Brito et al., 2014), however, their transport impacts the whole basin. During the wet season, Manaus emissions are the main anthropogenic influence on the aerosol population in the Amazon region (Andreae, 2007; Martin et al., 2010a). During the dry season, the wet deposition decreases whereas the condensation sink increases. That leads to an overall increase in aerosol concentration in the accumulation mode of about one order of magnitude even in remote areas (Artaxo et al., 2013).

The planetary boundary layer development displays a strong diel behavior, with a stable nocturnal layer and strong vertical mixing during the daytime. The vertical transport is enhanced in strong

convective situations when particles are lofted and entrained into the free troposphere. The stable nocturnal layer, on the other hand, traps the emissions near the surface; the impact can be more pronounced during the dry season as biomass burning usually starts at midday and continues into evening hours (Martin et al, 2010a). The boundary layer development is also different for the two different measurement sites, as the boundary layer develops more rapidly over the pasture area, with more efficient vertical mixing compared to the site enclosed by the rainforest.

2.4 Data analysis

All the available data from the NAIS were cleaned for a potential instrumental noise. The cleaning process was done visually using the particle and ion size distributions as surface plots. The non-reliable data were removed based on the guidelines introduced by Manninen et al. (2010). The NAIS data turned out to be unreliable during the measurements presented here mostly in the size range above 15 nm. Therefore, we decided to show data for the sizes up to 12 nm only in our analysis. We divided the measured ion and neutral particle concentrations into three sub size-ranges: cluster size-range (0.8 - 2 nm), intermediate size-range (2 - 4 nm), and large size-range (4 - 12 nm). Defining the lower and upper limits of the intermediate ion size range varies in the scientific literature (see Hirsikko et al., 2011 and references therein). The definition of using 2-4 nm as intermediate size-range allows for differentiating between new particle formation events and non-events when using ion measurements (Leino et al., 2016).

We observed an increase in the concentrations of the cluster ions in the NAIS starting from October 7, 2013 to January 21, 2014. By investigating the raw data files, this drift was observed to be due to too low currents in the sheath air filters. The sheath air filters are electrical filters, using corona needles to neutralize all the remaining ions, which leads to an over-estimation of ion concentrations. A correction factor of 1.8 was applied to account for this problem in the 4 smallest size channels of the NAIS (0.8-1.25 nm) for the data taken at the T0t site after the drift was observed. This increased level in the positive polarity of the natural ions continued when the NAIS was re-deployed at the T3 site. The cause was the same (too low a current in the sheath air filters). We consider the positive polarity of the natural charged ions in the NAIS at the T3 site unreliable, therefore the data, regarding the absolute concentrations, using the positive channel for the T3 site is not shown in this study. Additionally, the ion data from September 9-26, 2014 at the T3 site was considered unreliable and was also excluded from our analysis.

Rain-induced ion events were selected as the times when an ion burst coincided with the onset of precipitation. The median and the maximum (99^{th} percentile) ion concentrations were calculated during the periods when the rain intensity was >0 mm h^{-1}. In case of more than one rain-event per day, two separate rain-events were classified as such, if the start of the second one occurred more than an hour after the end of the first one. Any fluctuations in the rain intensity for a time period shorter than 1 hour were considered to be part of a single rain-event. We classified 962 rain-events at the T0t site and 221 rain-events at the T3 site.

The new particle formation event analysis from the ion spectrometer data, including the event classification and formation and growth rate calculations, followed the already well-defined guidelines (Kulmala et al., 2012). In the data analysis, the first step was to classify all available days into NPF event and non-event days according to methods introduced earlier by Hirsikko et al. (2007) and Manninen et al. (2010). The days that do not fulfill the criteria of an event or non-event day, are categorized as undefined days. However, no days were classified as undefined in this study.

The classification was performed manually through a visual inspection of daily contour plots of particle number size distributions. The second step in the analysis was to define the characteristics related to each NPF event, such as the particle growth rate (GR) and formation rate (J). The GRs were calculated for two different size bins (2-3 nm and 3-7 nm in particle diameter) using both ion and neutral particle data from the NAIS. The particle growth rate was determined by finding the times at which the maximum concentrations of ions/particles in each of these size ranges occurred. A fit between the points was then applied to resolve the growth rates. The particle formation rate was determined for the lower end of each size bin (2 and 3 nm) by taking the particle growth rate, condensation sink and coagulation sink into account.

3 Results

All the times mentioned below are local Manaus time (LT), which is Coordinated Universal Time (UTC) – 4 h.

3.1 Number concentrations of ions and particles at the two sites

An overview of the observed number concentrations of ions and particles together with the meteorological conditions at the two measurement sites is presented in Table 2.

When comparing the two measurement sites, the most apparent differences are: (i) the almost factor of 3 lower intermediate negative ion concentrations at the T3 site compared to the T0t site (6 cm^{-3} and 5 cm^{-3} during the wet and dry season, respectively, at T3; 17 cm^{-3} during both wet and dry season at T0t). This difference is likely to be caused by the enhanced formation of negative ions by the precipitation. (ii) By contrast, the large-sized ion concentrations were about a factor of 2 higher at the T3 site compared to the T0t site (20 cm^{-3} and 12 cm^{-3} during the wet and dry season, respectively, at T3; 8 cm^{-3} during both wet and dry season at T0t). (iii) Also, the intermediate and large-sized neutral particles were by about a factor of 3 higher at the T3 compared to the T0t site. These enhanced concentrations were probably due to a combination of stronger mixing of the boundary layer and the occurrence of NPF events at the T3 site.

The environmental variables were relatively similar at the two measurement sites, with higher average temperatures and lower average RH at the T3 site compared to the T0t site. The wind directions at both sites varied from the wet to the dry season. At T3, the air masses arrived, on

average, from 115° N during the wet season and from 95° N during the dry season. At T0t, the average wind direction changed from 94° during the wet season to 105 °N throughout the dry season (see Table 2).

3.1.1 Inside rainforest site (T0t)

At the T0t site, the negative cluster ion concentrations were very comparable during the wet (856 cm^{-3}) and the dry season (952 cm^{-3}). The positive cluster ion concentrations were by about a factor of 1.7 lower throughout both seasons compared to the negative ions (549 cm^{-3} (wet) and 537cm^{-3} (dry)). These values are comparable to those observed in several other locations (eg. urban Paris, Dos Santos et al. 2015; coastal Mace Head, Vana et al. 2008 and Finokalia, Kalvitis et al. 2012; Puy de Dome, Rose et al. 2016).

The ion concentrations in the intermediate size range (2-4 nm) were a factor of 2 higher in the positive polarity compared to the negative polarity both in the wet and in the dry season (17 cm^{-3} (-) and 34 cm^{-3} (+) during the wet season; 17 cm^{-3} (-) and 34 cm^{-3} (+) during the dry season). We observed the same concentrations in the large size range on the other hand in both polarities and both seasons (8 cm^{-3}). The neutral particle concentrations were higher in the intermediate (2-4 nm) size range compared to the large (4-12 nm) size range, being very similar in the wet and dry season. The characteristics of the wet and the dry season in the Amazon (Rissler et al. 2006, Martin et al. 2010a) can be observed in the concentrations of the negative ions as shown in Figure 2. The negative ion concentrations were decreasing from April to September and increasing between September and February. Most likely, the local biomass burning during the dry season increased the ion concentrations. During the wet season, the ion concentrations decreased most likely due to wet deposition and reduced source strengths.

We observed a similar diel pattern for both the wet and the dry season for the neutral particles as shown in Figure 3. The concentrations in both size ranges increase at around 06:00 – 09:00 during the wet season. This effect was less pronounced in the dry season. A clear decrease in neutral particle concentrations during evening times (after 17:00) can be observed.

3.1.2. Pasture site (T3)

As shown in Table 2, cluster ion concentrations at the T3 site were typically higher during the wet season (1300 cm^{-3}) than the dry season (890 cm^{-3}). Similar, high ion concentrations were reported in an Australian rainforest in Tumbarumba (Suni et al. 2008) and in a wetland site in Abisko (Svennigsson et al., 2008). Those experiments showed concentrations of ~2400 (1700) cm^{-3} for negative (positive) ions. The median negative ion concentrations in the intermediate and large size ranges (2 - 4 nm and 4 - 12 nm) were very similar during the wet season (6 cm^{-3}, 20 cm^{-3}) and the dry season (5 cm^{-3}, 12 cm^{-3}). The neutral particle concentrations were also very similar in both seasons at the T3 site. The median total concentrations measured by the ultrafine MAOS CPC (>10

nm) were observed to be more than a factor of 2 higher in the dry season than in the wet season (928 cm^{-3} versus 2000 cm^{-3}). This difference is most likely due to the enhanced biomass burning during the dry season. The average temperatures and the average relative humidity were very similar in both seasons.

The PSM measurements were performed during the dry season only. In total, 38 days of PSM data were included in this study and the results are shown in Figure 4. The PSM was used in scanning mode but, due to the challenging environmental conditions, only data measured at the highest supersaturation (total particle concentration at >1.5 nm) is shown. The PSM data showed a similar diel pattern as the cluster ion concentrations measured by the NAIS (see Fig. 9), with higher median concentrations observed during the early morning (03:00-06:00), a dip in concentrations during the early afternoon (12:00-15:00), and then elevated median concentrations again in the evening (18:00-24:00). This could be explained by the Carnegie curve (Harrison, R. G. and Carslaw, K. S., 2003), which manifests as a diel variation in the ionospheric potential.

3.2 Rain-induced ion formation events

While no NPF events were observed within the rainforest at site T0t, rain-induced ion burst events (hereafter, rain-events) were common and observed during 264 out of the 384 measurement days. Since multiple rain episodes could occur in a single day, each rain-event was investigated separately, giving a total of 962 rain-events at T0t site and 221 at the T3 site.

Figure 5 shows an example of multiple rain-events that took place during January 24, 2013 (wet season). The negative ion concentrations in the cluster size range of 0.8 – 2 nm increased during the precipitation from about 1000 cm^{-3} to 1500 cm^{-3}. The positive cluster ion concentrations on the other hand decreased during the precipitation episode from 1000 cm^{-3} to about 500 cm^{-3}. The intermediate (2 - 4 nm) ion concentrations showed an increase in both polarities, although the buildup was more pronounced for the negative intermediate-sized ions. In the intermediate size range, the concentrations of negative ions reached up to 3000 cm^{-3}, while during the same precipitation event, the positive intermediate ion concentrations only rose to 200 cm^{-3}. A similar feature for 2-8 nm-sized negative ions during rain-events has also been reported for an Australian rainforest (Suni et al. 2008). In that study, the positive ion concentrations increased only in the 3-7 nm size range and decreased in the 1-3 nm size range during the precipitation episodes. These rain-induced ion bursts are thought to be a result of a balloelectric effect, in which splashing water produces intermediate ions, such that the negative ions are smaller in size than the positive ions (Horrak et al., 2005, Hirsikko et al., 2007, Tammet et al., 2009).

The duration of the 962 rain-events in our study varied from a couple of minutes to 22 hours, with over half of the rain-events lasting for two hours or less. The statistics of the rain-event frequency from the T0t measurement site are shown in Figure 6. The bars show the mean number of days with

and without rain and the black line shows the median total average precipitation per month. Figure 6 shows that rain-events occurred in both seasons. However, the number of days without rain increased during the dry season (July to December).

Figure 7 shows the correlation between the maximum negative ion concentration and the median rain intensity during each rain-event. While no clear connection between these two quantities was found, two specific features are apparent: at the site within the canopy (T0t), the highest cluster and intermediate ion concentrations occurred almost entirely in correlation with rather strong rain intensities, whereas at the pasture site (T3) almost no increase in negative ion concentrations in any size range during precipitation periods could be observed.

The rain-events were also evident in the total particle concentration measured by the NAIS, as depicted in Figure 8. In this example, the rain intensity peaks twice, about 40 mm h^{-1} at ~09:00 followed by a second peak of 10 mm h^{-1} at ~11:00. The ion and particle concentrations measured by the NAIS increased and decreased almost simultaneously with the increase and decrease of the precipitation rate. Additionally, the DMPS data showed an appearance of nucleation mode particles between 6 and 10 nm, also following the onset of the rain. Please note, that the DMPS was sampling at a height of 60 m, which is well above the rainforest canopy. The concentration of 6-10 nm particles increased by a factor of 4 during the rain-event, as compared to a background concentration of 5 cm^{-3} in the absence of precipitation. The 10-20 nm particle concentrations first showed a drop, followed by an increase up to ~35 cm^{-3}. The maximum concentrations of the 10 – 20 nm particles appeared about 4 hours after the short-term increase of the 6-10 nm particles.

The appearance of 6-10 nm particles and their peak concentration could present a similar scenario as observed in Wang et al (2016). They reported a production of small aerosol particles as a result of new particle formation in cloud outflow regions, with further transport into the boundary layer due to strong convection during precipitation events in the Amazon. Wang et al. (2016) noted that the <20 nm particle concentrations decreased very rapidly. We suggest the process that we observe is a local one because the production of ions was observed to only last for the duration of the precipitation.

3.3 New particle formation events at T3

We observed no NPF events during the dry season. During the wet season, on 9% of the days, we did observe NPF events. A similar event frequency has been observed in the Finnish boreal forest environment during the autumn as an example (Kontkanen et al., 2017). An earlier study by Backman et al. (2012) showed that in the metropolitan area of São Paulo (population 20 million), Brazil, NPF events occurred on 11% of the days. Zhou et al. (2002) observed an ultrafine particle mode in central Amazonia on 18% of the measurement days.

We selected all eight NPF event days to characterize the behavior of ions and aerosol particles during the bursts of particle formation. A comparison of the diel cycle for particles and ions between NPF and non-event days is shown in Figure 9. The cluster ions showed a clear diel cycle with higher concentrations in the morning and evening for both NPF and non-event days. An increase in the concentrations of intermediate and large ions (2-4 nm and 4-12 nm) occurred during NPF event days, which was due to the growth of the ions from the cluster ion size range (0.8-2 nm) to larger sizes. The intermediate neutral particle concentrations increased at around 09:00, suggesting an onset of NPF after the sunrise when the boundary layer begins to grow and turbulent mixing starts. On non-event days these particles showed the highest concentrations after the sunrise (06:00) and the sunset (18:00). The total particle concentration measured by the MAOS CPC showed a clear concentration increase on NPF event days, starting from 10:00, which clearly indicates that the particles had grown from smaller sizes into the 10 nm detection limit of the MAOS CPC. No clear diel pattern in the MAOS CPC measurements was visible on non-event days.

The type of NPF events that we observed are likely of regional nature, requiring relatively homogeneous air masses for at least a few hours (Vana et al., 2004; Manninen et al., 2010). The most likely explanations for why no new particle formation events were observed at the T0t site are: (i) either the lack of SO_2 sources for forming sulfuric acid or (ii) that the sampling at the less polluted T0t site was performed within the rainforest, where mixing with the atmospheric boundary layer above is hindered. The gaps, or fluctuations, in the usually distinct NPF shape in time-size-concentration plots could be caused by some degree of heterogeneity in the measured air masses. All NPF events occurred during the daytime, starting at around 08:00 - 09:00, 2 – 3 hours after sunrise. All NPF events took place during the wet season, which might be due to the lower condensation sink at this time of the year, as shown in Table 1. The median sulfuric acid concentrations, as measured by a quadrupole HOx CIMS (Martin et al, 2016, supplementary material), were about $9x10^5$ cm^{-3} for both NPF event and non-event days. Similar sulfuric acid concentrations were reported for the Finnish boreal forest measurements in autumn, where about 12% of the days were classified as NPF event days (Kontkanen et al., 2017).

Back trajectories using HYSPLIT (http://ready.arl.noaa.gov/hypub-bin/trajtype.pl?runtype=archive; Rolph et al., 2017) were calculated using Global Data Assimilation System model data produced by the National Centers for Environmental Prediction (NCEP), and showed a clear difference in the air mass origins arriving at the measurement site during the NPF event and non-event days. The back trajectories were calculated as ensembles for 24 hours to arrive at 13:00 UTC (09:00 local time) at 500m a. s. l. The back-trajectories were calculated on NPF event days and for each day prior to and following an NPF event day. If an NPF event occurred on two consecutive days, the day after both events was used for the non-event day back-trajectory calculations. On non-event days, the 50^{th} percentile of air masses originated from 2. 9°S, 58.6°W and 545 m.a.s.l., a location upstream of the Amazon river. On NPF event days, the back-trajectory calculations show an origin at 2.5°S, 58.5°W and 602.5 m a. s. l.; further north, which is an area with dense rainforest. The results of the back-trajectory calculations are shown in Figure 10.

Figure 11 shows an example of an NPF event observed at the pasture site (T3), displaying MAOS SMPS data, NAIS total particle concentrations, and NAIS negative ion concentrations. The intermediate ion concentrations increased during this NPF event, starting at 08:00, with a continuous growth, reaching the smallest size channel of the MAOS SMPS at 10:00 (blue dashed line in panel d) of Figure 11). The same can be observed in the large particle and ion (4-12 nm) channel from the NAIS (red and black lines respectively).

Table 3 shows a comparison of the median particle and ion concentrations (25^{th} – 75^{th} percentiles in brackets), as well as the condensation sink, for the time window 08:00-12:00 comparing the NPF event and non-event days. The condensation sink was clearly lower on NPF event days (0.0018 s^{-1}) than on non-event days (0.003 s^{-1}), and the median concentration of intermediate (2-4 nm) ions and neutral particles was 1.3 times higher on NPF event days. The ion concentrations in the large size range were about a factor of 1.7 higher and neutral particle concentrations in the same size range were 2.4 times higher during the time of NPF compared to non-event days.

We also compared environmental variables, including the temperature, relative humidity and wind direction. No precipitation during any of the classified NPF events was observed, but on two classified NPF event days, precipitation periods were observed before or after the NPF events (starting at 06:00 and 17:00 respectively). The median temperature and RH were about the same for NPF event and non-event days, whereas the median wind direction changed (83°N on event days and 105.5°N during non-event days), consistent with the results from the back-trajectory analysis.

Table 4 shows the calculated growth rates, particle formation rates, and condensation sinks for each classified NPF event day. Note that here, the condensation sink was calculated for the time of the event, whereas the numbers in Tables 2 and 3 are for the whole day. The quantiles of both particle formation rate and growth rate were determined for two different size ranges (2-3 nm and 3-7 nm), and calculated separately for the ion and particle data. The results show considerably lower ion formation rates compared with neutral particle formation rates, consistent with observations made at most other continental sites (Manninen et al., 2010; Hirsikko et al., 2011). The growth rates of particles and ions were comparable to each other and typically smaller for the 2-3 nm size range than the 3-7 nm size range. An increase in the particle and ion growth rate with an increasing particle size has previously been reported at a few other sites (see Häkkinen et al., 2013, and references therein). We observed two regimes when looking at the neutral 3-7 nm growth rate. On 3 days, the growth rate was about 2 nm h^{-1}, with sulfuric acid concentrations of about $2x10^6$ cm^{-3}. According to theoretical calculations about 10^7 cm^{-3} of sulfuric acid molecules can account for 1 nm h^{-1} (Nieminen et al., 2010). It is most likely that other compounds are contributing to the growth. Other NPF event days showed growth rates of about 14 nm h^{-1} for the same 3-7 nm size range, and the sulfuric acid concentration was even lower (about $6x10^5$ cm^{-3}). These growth rates are most likely driven by organic compounds (Tröstl et al., 2016). Tröstl et al. (2016) calculated that about 10^6-10^7 cm^{-3} of highly oxidized organic compounds are required to explain a growth rate of about 10 nm h^{-1}.

4 Summary and Conclusions

We performed direct measurements of atmospheric new particle formation (NPF) events in the Amazon region with state-of-the-art aerosol instrumentation. The measurement campaigns were performed at two observation sites (T0t and T3) in the vicinity of Manaus in Brazil. One site was located within the rainforest (T0t), providing long-term (September 2011 to January 2014) measurement data, to complement data from a pasture site (T3, January to October 2014).

No NPF events were observed at the T0t site during the long-term measurement period. However, we observed rain-induced ion and particle burst events ("rain-events") inside the rainforest during 264 of the 384 days. Concentrations of 2 - 4 nm and 4 - 12 nm ions and total particles were enhanced by up to 3 orders of magnitude during such rain-events (~10^4-10^5 cm^{-3}) at T0t site. The rain-events occurred throughout the year, but the number of days with precipitation was the highest from December to June corresponding to the wet season. Multiple rain-events could occur during the same day, totaling 1491 rain-events in 643 rainy days for both sites together. The duration of the rain-events ranged from a couple of minutes to 22 hours, but over 50% of the events lasted for <2 hours. During the rain-events, 0.8 - 2 nm and 2 - 4 nm negative ions increased more than the same-size positive ions. The production of small (0.8 - 2 nm) and intermediate negative ions (2 - 4 nm) during rain-events reached a maximum of 10^5 cm^{-3} at the T0t site.

At the pasture site, we observed a clear diel pattern in the cluster ion concentration during both the wet and the dry season, with higher concentrations observed during the morning and evening. The PSM observations showed a similar diel cycle for particles >1.5 nm, with higher concentrations in the early morning, a dip in the afternoon, and an increase again in the evening after sunset. The diel cycle was less pronounced inside the rainforest, indicating that the rainforest canopy hinders vertical mixing.

We observed eight NPF events showing particle growth at the pasture site during January to March 2014. The formation rates were considerably higher for neutral particles than ions during these NPF events. The growth rates of newly-formed ions and particles were comparable to each other and showed a clear increase with increasing size in the sub-20 nm size range. We found two different regimes for growth rates in the 3-7 nm size range; 3 out of 8 NPF days showed a growth rate of about 2 nmh^{-1}, and on 4 out of 8 NPF days, a growth rate of about 14 nmh^{-1} was observed. The sulfuric acid concentrations were similar for both NPF event and non-event days (approx. 9x10^5 cm^{-3}). Most likely the observed growth for all NPF events is driven by highly oxidized organic compounds (Tröstl et al., 2016).

The back-trajectory calculations using HYSPLIT did not show any clear difference between the days with high and low growth rates. Nevertheless, there was a clear difference in air mass origin between the days with NPF events when back-trajectories originated from the rainforest, and non-event days when back-trajectories originated from the Amazon river. As observed in SMPS

measurements, particles grew to the sizes of around 60 nm during all the NPF events, above which they are able to act as cloud condensation nuclei (McFiggans et al, 2006; Andreae and Rosenfeld, 2008; Kerminen et al. 2012). There were clear differences in the median cluster and intermediate ion concentrations between the NPF event and non-event days for the local time window of 08:00-12:00. For NPF event days, the median intermediate ion and particle concentration was higher by a factor of 1.3 compared to non-event days. The condensation sink was also lower on the NPF event days (0.0016 s^{-1}) than on non-event days (0.003 s^{-1}). There were no NPF events observed during the dry season, when it is likely that the condensation sink is too high for new particle formation.

Acknowledgements

We acknowledge the Academy of Finland Centre of Excellence program (grant no. 272041). We acknowledge the Atmospheric Radiation Measurement (ARM) Climate Research Facility, a user facility of the United States Department of Energy, Office of Science, sponsored by the Office of Biological and Environmental Research, and support from the Atmospheric System Research (ASR) program of that office. D.W. wishes to acknowledge the Austrian Science Fund (FWF, grant no J-3951). P Artaxo acknowledges FAPESP project 2013/05014-0 and CNPq for funding. We thank field support from Alcides Ribeiro, Bruno Takeshi and Fabio Jorge. We acknowledge logistical support from the LBA Central Office, at the INPA – Instituto Nacional de Pesquisas da Amazonia.

References

Aalto, P., Hämeri, K., Becker, E., Weber, R., Salm, J., Mäkelä, J. M., Hoell, C., O'Dowd, C. D., Karlsson, H., Hansson, H. C., Väkevä, M., Koponen, I. K., Buzorius, G., and Kulmala, M., Physical characterization of aerosol particles during nucleation events, Tellus B, 53:4, 344-358, 2001, doi: 10.1034/j.1600-0889.2001.530403.x.

Andreae, M. O.: Aerosols before pollution, Science, 315, 50–51, 2007.

Andreae, M. O., and Rosenfeld, D.: Aerosol-cloud-precipitation interactions. Part 1. The nature and sources of cloud-active aerosols, Earth-Sci. Rev., 89, 13-41, 2008, Doi: 10.1016/j.earscirev.2008.03.001.

Andreae, M. O., Acevedo, O. C., Araùjo, A., Artaxo, P., Barbosa, C. G. G., Barbosa, H. M. J., Brito, J., Carbone, S., Chi, X., Cintra, B. B. L., da Silva, N. F., Dias, N. L., Dias- Júnior, C. Q., Ditas, F., Ditz, R., Godoi, A. F. L., Godoi, R. H. M., Heimann, M., Hoffmann, T., Kesselmeier, J., Könemann, T., Krüger, M. L., Lavric, J. V., Manzi, A. O., Lopes, A. P., Martins, D. L., Mikhailov, E. F., Moran-Zuloaga, D., Nelson, B. W., Nölscher, A. C., Santos Nogueira, D., Piedade, M. T. F., Pöhlker, C.,

601 Pöschl, U., Quesada, C. A., Rizzo, L. V., Ro, C.-U., Ruckteschler, N., Sá, L. D. A., de Oliveira Sá,
602 M., Sales, C. B., dos Santos, R. M. N., Saturno, J., Schöngart, J., Sörgel, M., de Souza, C. M., de
603 Souza, R. A. F., Su, H., Targhetta, N., Tóta, J., Trebs, I., Trumbore, S., van Eijck, A., Walter, D.,
604 Wang, Z., Weber, B., Williams, J., Winderlich, J., Wittmann, F., Wolff, S., and Yáñez-Serrano, A.
605 M.: The Amazon Tall Tower Observatory (ATTO): overview of pilot measurements on ecosystem
606 ecology, meteorology, trace gases, and aerosols, Atmos. Chem. Phys., 15, 10723–10776, 2015,
607 doi:10.5194/acp-15- 10723-2015.
608
609 Artaxo, P., Rizzo, L. V., Brito, J. F., Barbosa, H. M. J., Arana, A., Sena, E. T., Cirino, G. G., Bastos,
610 W., Martin, S. T., and Andreae, M. O.: Atmospheric aerosols in Amazonia and land use change: from
611 natural biogenic to biomass burning conditions, Faraday Discuss., 165, 203–235, 2013.
612
613 Asmi, E., Sipilä, M., Manninen, H. E., Vanhanen, J., Lehtipalo, K., Gagné, S., Neitola, K., Mirme,
614 A., Mirme, S., Tamm, E., Uin, J., Komsaare, K., Attoui, M., and Kulmala, M.: Results of the first air
615 ion spectrometer calibration and intercomparison workshop, Atmos. Chem. Phys., 9, 141-154, 2009,
616 doi:10.5194/acp-9-141-2009.
617
618 Backman, J., Rizzo, L. V., Hakala, J., Nieminen, T., Manninen, H. E., Morais, F., Aalto, P. P., Siivola,
619 E., Carbone, S., Hillamo, R., Artaxo, P., Virkkula, A., Petäjä, T., and Kulmala, M.: On the diurnal
620 cycle of urban aerosols, black carbon and the occurrence of new particle formation events in
621 springtime São Paulo, Brazil, Atmos. Chem. Phys., 12, 11733-11751, 2012, doi:10.5194/acp-12-
622 11733-2012.
623
624 Dunne, E., Gordon, H., Kürten, A., Almeida, J., Duplissy, J., Williamson, C., Ortega, I. K., Pringle,
625 J.K., Adamov, A., Baltensperger, U., Barmet, P., Benduhn, F., Bianchi, F., Breitenlechner, M.,
626 Clarke, A., Curtius, J., Dommen, J., Donahue, N. M., Ehrhart, S., Flagan, R. C.,Franchin, A., Guida,
627 R., Hakala, J., Hansel, A., Heinritzi, M., Jokinen, T., Kangasluoma, J., Kirkby, J., Kulmala, M., Kupc,
628 A., Lawler, M. J., Lehtipalo, K., Makhmutov, V., Mann, G., Mathot, S., Merikanto, J., Miettinen, P.,
629 Nenes, A., Onnela, A., Rap, A., Reddington, C. L. S., Riccobono, F., Richards, N. D. A.,Rissanen,
630 M. P., Rondo, L., Sarnela, N., Schobesberger, S., Sengupta, K., Simon, M., Sipilä, M., Smith, J. N.,
631 Stozkhov, Y., Tomé, A., Tröstl, J., Wagner, P. E., Wimmer, D., Winkler, P. M., Worsnop, D. R., and
632 Carslaw K. S., Global atmospheric particle formation from CERN CLOUD measurements, Science,
633 354: 6316, 2016.
634
635 Dos Santos, V. N., Herrmann, E., Manninen, H. E., Hussein, T., Hakala, J., Nieminen, T., Aalto, P.
636 P., Merkel, M., Wiedensohler, A., Kulmala, M., Petäjä, T., and Hämeri, K., Atmos. Chem. Phys., 15;
637 23:13717-13737, 2015, doi: 10.5194/acp-15-13717-2015.
638
639 Häkkinen, S. A. K., Manninen, H. E., Yli-Juuti, T., Merikanto, J., Kajos, M. K., Nieminen, T.,
640 D'Andrea, S. D., Asmi, A., Pierce, J. R., Kulmala, M. and Riipinen, I.: Semi-empirical
641 parameterization of size-dependent atmospheric nanoparticle growth in continental environments,
642 Atmos. Chem. Phys., 13, 15: 7665-7682, 2013, doi: 10.5194/acp-13-7665-2013.
643

644 Harrison, R. G., and Carslaw, K. S., Ion-Aerosol-cloud processes in the lower atmosphere, Rev.
645 Geophys., 41, 3 / 1012, 2003, doi:10.1029/2002RG000114.
646
647 Hirsikko, A, Laakso, L, Horrak, U, Aalto, P. P., Kerminen, V.-M., and Kulmala, M., Annual and size
648 dependent variation of growth rates and ion concentrations in boreal forest, Bor. Environ. Res., 10,
649 357-369, 2005.

650

651 Hirsikko, A., Bergman, T., Laakso, L., Dal Maso, M., Riipinen, I., Hõrrak, U., and Kulmala, M.,
652 Identification and classification of the formation of intermediate ions measured in boreal forest,
653 Atmos. Chem. Phys., 7, 201-210, 2007.

654 Hirsikko, A., Nieminen, T., Gagné, S., Lehtipalo, K., Manninen, H. E., Ehn, M., Hõrrak, U.
655 Kerminen, V-M., Laakso, L., McMurry, P. H., Mirme, A., Mirme, S., Petäjä, T., Tammet, H.,
656 Vakkari, V., Vana, M., and Kulmala, M. Atmospheric ions and nucleation: a review of observations,
657 Atmos. Chem. Phys., 11, 767-798, 2011, doi: 10.5194/acp-11-767-2011.

658

659 Hoppel, W. A., Theory of the electrode effect, J. Atmos. Terr. Phys., Vol. 22, 1967.

660
661 Hõrrak, U., Salm, J., and Tammet, H., Bursts of intermediate ions in atmospheric air, J. Geophys.
662 Res.: Atmos., 103: 13909-13915, 1998, doi: 10.1029/97JD01570.
663
664 Hõrrak, U., Tammet, H., Aalto, P. P., Vana, M., Hirsikko, A.,
665 Laakso, L., and Kulmala, M.: Formation of charged particles
666 associated with rainfall: atmospheric measurements and lab experiments,
667 Rep. Ser. Aerosol Sci., 80, 180–185, 2006.
668
669 Kalivitis, N., Stavroulas, I., Bougiatioti, A., Kouvarakis, G., Gagné, S., Manninen, H. E., Kulmala,
670 M., and Mihalopoulos, N.: Night-time enhanced atmospheric ion concentrations in the marine
671 boundary layer, Atmos. Chem. Phys., 12, 3627-3638, 2012, doi:10.5194/acp-12-3627-2012.
672
673 Kangasluoma J., Kuang C., Wimmer D., Rissanen M. P., Lehtipalo K., Ehn M., Worsnop, D. R.,
674 Wang, J., Kulmala M., and Petäjä T., Sub-3nm particle size and composition dependent response of
675 a nano-CPC battery, Atmos. Meas. Tech., 7, 689–700, 2014, doi:10.5194/amt-7-689-2014.
676
677 Kerminen, V-M, Paramonov, M., Anttila, T., Riipinen, I., Fountoukis, C, Korhonen, H., Asmi, E.,
678 Laakso, L., Lihäväinen, H., Swietlicki, E., Svenningsson, B., Asmi, A., Pandis, S. N, Kulmala, M.,
679 and Petäjä, T., Cloud condensation nuclei production associated with atmospheric nucleation: a
680 synthesis based on existing literature and new results, Atmos. Chem. Phys., 12, 24: 12037-12059,
681 2012, doi: 10.5194/acp-12-12037-2012.
682
683 Kontkanen, J., Lehtipalo, K., Ahonen, L., Kangasluoma, J., Manninen, H. E., Hakala, J., Rose, C.,
684 Sellegri, K., Xiao, S., Wang, L., Qi, X., Nie, W., Ding, A., Yu, H., Lee, S., Kerminen, V.-M., Petäjä,
685 T.., and Kulmala, M., Measurements of sub-3 nm particles using a particle size magnifier in different

686 environments: from clean mountain top to polluted megacities, Atmos. Chem. Phys., 2163–2187,
687 2017, doi:10.5194/acp-17-2163-2017.
688 Kulmala, M., Vehkämäki, H, Petäjä, T., Dal Maso, M., Lauri, A, Kerminen, VM, Birmili, and
689 McMurry, PH., Formation and growth rates of ultrafine atmospheric particles: a review of
690 observations, J. Aerosol Sci., 35,143-176, 2004.
691
692 Kulmala, M., Petäjä, T., Nieminen, T., Sipilä, M., Manninen, H. E., Lehtipalo, K., Dal Maso, M.,
693 Aalto, P. P., Junninen, H., Paasonen, P., Riipinen, I., Lehtinen, K. E. J., Laaksonen, A., and Kerminen,
694 V.-M.: Measurement of the nucleation of atmospheric aerosol particles, Nat. Protoc., 7, 1651–1667,
695 2012.
696
697 Kulmala, M., Kontkanen, J., Junninen, H., Lehtipalo, K., Manninen, HE, Nieminen, T., Petäjä, T.,
698 Sipilä, M., Schobesberger, S., Rantala, P., Franchin, A, Jokinen, T., Järvinen, E., Äijala, M.,
699 Kangasluoma, J., Hakala, J., Aalto, P. P., Paasonen, P., Mikkilä, J., Vanhanen, J., Aalto, J., Hakola,
700 H., Makkonen, U., Ruuskanen, T., Mauldin, R. L., III, Duplissy, J., Vehkämäki, H., Back, J.,
701 Kortelainen, A., Riipinen, I., Kurten, T., Johnston, M. V., Smith, J. N. Ehn, M., Mentel, T. F.,
702 Lehtinen, K. E. J., Laaksonen, A., Kerminen, V.-M., and Worsnop, D. R., Direct Observations of
703 Atmospheric Aerosol Nucleation, Science, 339, 943, 2013.
704
705 Kulmala, M., Petäjä, T. Ehn, M., Thornton, J., Sipilä, M., Worsnop, D. R., and Kerminen, V. -M.,
706 Chemistry of Atmospheric Nucleation: On the Recent Advances on Precursor Characterization and
707 Atmospheric Cluster Composition in Connection with Atmospheric New Particle Formation, Annu.
708 Rev. Phys. Chem., 65, 21–37, 2014.
709
710 Kulmala, M., Luoma, K., Virkkula, A, Petäjä, T., Paasonen, P., Kerminen, V.-M. Nie, W., Qi, X.,
711 Shen, Y., Chi, X., and Ding, A., On the mode-segregated aerosol particle number concentration load:
712 contributions of primary and secondary particles in Hyytiala and Nanjing
713 Bor. Environ. Res., 21, 319-331, 2016.
714
715 Leino, K., Nieminen, T., Manninen, H. E., Petäjä, T., Kerminen, V.-M., and Kulmala, M.,
716 Intermediate ions as a strong indicator of new particle formation bursts in a boreal forest, Bor.
717 Environ. Res., 21, 274-286, 2016.
718
719 Lelieveld J., Butler, T. M., Crowley, J. N., Dillon, T. J., Fischer, H., Ganzeveld, L., Harder, H.,
720 Lawrence, M. G., Martinez, M., Taraborrelli, D., and Williams, J., Atmospheric oxidation capacity
721 sustained by a tropical forest, Nature 452, 737-740, 2008.
722
723 Manninen, H. E., Nieminen, T., Asmi, E., Gagné, S., Häkkinen, S., Lehtipalo, K., Aalto, P., Vana,
724 M., Mirme, A., Mirme, S., Hõrrak, U., Plass-Dülmer, C., Stange, G., Kiss, G., Hoffer, A., Törő, N.,
725 Moerman, M., Henzing, B., de Leeuw, G., Brinkenberg, M., Kouvarakis, G. N., Bougiatioti, A.,
726 Mihalopoulos, N., O'Dowd, C., Ceburnis, D., Arneth, A., Svenningsson, B., Swietlicki, E., Tarozzi,
727 L., Decesari, S., Facchini, M. C., Birmili, W., Sonntag, A., Wiedensohler, A., Boulon, J., Sellegri,
728 K., Laj, P., Gysel, M., Bukowiecki, N., Weingartner, E., Wehrle, G., Laaksonen, A., Hamed, A.,
729 Joutsensaari, J., Petäjä, T., Kerminen, V.-M., and Kulmala, M.: EUCAARI ion spectrometer
730 measurements at 12 European sites – analysis of new particle formation events, Atmos. Chem. Phys.,
731 10, 7907-7927, 2010, doi:10.5194/acp-10-7907-2010.
732

733 Manninen, H. E., Mirme, S., Mirme, A., Petäjä, T., and Kulmala, M.: How to reliably detect molecular
734 clusters and nucleation mode particles with Neutral cluster and Air Ion Spectrometer (NAIS), Atmos.
735 Meas. Tech., 9, 3577-3605, 2016, doi:10.5194/amt-9-3577-2016.
736
737 Martin, S. T., Andreae, M. O., Artaxo, P., Baumgardner, D., Chen, Q., Goldstein, A. H., Guenther,
738 A., Heald, C. L., Mayol-Bracero, O. L., McMurry, P. H., Pauliquevis, T., Poeschl, U., Prather, K. A.,
739 Roberts, G. C., Saleska, S. R., Silva Dias, M. A., Spracklen, D. V., Swietlicki, E., and Trebs, I.,
740 Sources and properties of Amazonian aerosol particles, Rev. Geophys., 48, RG2002, 2010a, doi:
741 10.1029/2008RG000280.
742
743 Martin, S. T., Andreae, M. O., Althausen, D., Artaxo, P., Baars, H., Borrmann, S., Chen, Q., Farmer,
744 D. K., Guenther, A., Gunther, S. S., Jimenez, J. L., Karl, T., Longo, K., Manzi, A.,
745 Müller, T., Pauliquevis, T., Petters, M. D., Prenni, A. J., Pöschl, U., Rizzo, L. V., Schneider, J., Smith,
746 J. N., Swietlicki, E., Tota, J., Wang, J., Wiedensohler, A., and Zorn, S. R.: An overview of the
747 Amazonian Aerosol Characterization Experiment 2008 (AMAZE-08), Atmos. Chem. Phys., 10,
748 11415–11438, 2010b, doi:10.5194/acp-10-11415-2010.
749 Martin, S. T., Artaxo, P., Machado, L. A. T., Manzi, A. O., Souza, R. A. F., Schumacher, C., Wang,
750 J., Andreae, M. O., Barbosa, H. M. J., Fan, J., Fisch, G., Goldstein, A. H., Guenther, A., Jimenez, J.
751 L., Pöschl, U., Silva Dias, M. A., Smith, J. N., and Wendisch, M.: Introduction: Observations and
752 Modeling of the Green Ocean Amazon (GoAmazon2014/5), Atmos. Chem. Phys., 16, 4785-4797,
753 2016, doi:10.5194/acp-16-4785-2016.
754
755 Martin, S. T., Artaxo P., Machado, L., Manzi, A. O., Souza, R. A. F., Schumacher, C., Wang, J.,
756 Biscaro, T., Brito, J., Calheiros, A., Jardine, K., Medeiros, A., Portela, B., de Sá, S. S., Adachi, K.,
757 Aiken, A. C., Albrecht, R., Alexander, L., Andreae, M. O., Barbosa, H. M. J., Buseck, P., Chand, D.,
758 Comstock, J. M., Day, D. A., Dubey, M., Fan, J., Fast, J., Fisch, G., Fortner, E., Giangrande, S.,
759 Gilles, M., Goldstein, A. H., Guenther, A., Hubbe, J., Jensen, M., Jimenez, J. L., Keutsch, F. N., Kim,
760 S., Kuang, C., Laskin, A., McKinney, K., Mei, F., Miller, M., Nascimento, R., Pauliquevis, T.,
761 Pekour, M., Peres, J., Petäjä, T, Pöhlker, C., Pöschl, U., Rizzo, L., Schmid, B., Shilling, J. E., Silva
762 Dias, M. A., Smith, J. N., Tomlinson, J. M., Tóta, J., and Wendisch, M., The Green Ocean Amazon
763 Experiment (GoAmazon2014/5) observes pollution affecting gases, aerosols, clouds and rainfall over
764 the rain forest, Bull. Am. Meteor. Soc., 2017, doi:10.1175/BAMS-D-15-00221.1.
765
766 Mather, J. H., and Voyles, J. W.: The ARM Climate Research Facility: A review of structure and
767 capabilities, Bull. Am. Meteor. Soc., 94, 377–392, 2013.
768
769 McFiggans, G, Artaxo, P., Baltensperger, U., Coe, H., Facchini, M. C., Feingold, G., Fuzzi, S., Gysel,
770 M., Laaksonen, A., Lohmann, U., Mentel, T. F., Murphy, D. M., O'Dowd, C. D., Snider, J. R.) and
771 Weingartner, E., The effect of physical and chemical aerosol properties on warm cloud droplet
772 activation, Atmos. Chem. Phys, 6, 2593-2649, 2006.
773
774 Merikanto, J., Spracklen, D. V., Mann, G. W., Pickering, S. J., and Carslaw, K. S.: Impact of
775 nucleation on global CCN, Atmos. Chem. Phys., 9, 8601-8616, 2009, doi:10.5194/acp-9-8601-2009.
776

Nieminen, T., Yli-Juuti, T., Manninen, H. E., Petäjä, T., Kerminen, V.-M., and Kulmala, M.: Technical note: New particle formation event forecasts during PEGASOS–Zeppelin Northern mission 2013 in Hyytiälä, Finland, Atmos. Chem. Phys., 15, 12385-12396, 2015, doi:10.5194/acp-15-12385-2015.

Nieminen, T., Lehtinen, K. E. J., and Kulmala, M., Sub-10 nm particle growth by vapor condensation - effects of vapor molecule size and particle thermal speed, Atmos. Chem. Phys., 10, 9773-9779, 2010, DOI: 10.5194/acp-10-9773-2010.

Rose, C., Sellegri, K., Velarde, F., Moreno, I., Ramonet, M., Weinhold, K., Krejci, R. Ginot, P., Andrade, M., Wiedensohler, A., and Laj, P., Frequent nucleation events at the high altitude station of Chacaltaya (5240 m a.s.l.), Bolivia, Atmos. Environ., 102, 18-29, DOI: 10.1016/j.atmosenv.2014.11.015, 2015.

Rolph, G., A. Stein and B. Stunder, Real-time Environmental Applications and Display sYstem: READY, Environmental Modelling & Software, 95, 210-228, 2017, doi:10.1016/j.envsoft.2017.06.025.

Tammet, H., Hõrrak, U., and Kulmala, M.: Negatively charged nanoparticles produced by splashing of water, Atmos. Chem. Phys., 9, 357-367, 2009, doi:10.5194/acp-9-357-2009.

Tröstl, J., Chuang, W. K., Gordon, H., Heinritzi, M., Yan, C., Molteni, U., Ahlm, L., Frege, C., Bianchi, F., Wagner, R., Simon, M., Lehtipalo, K., Williamson, C., Craven, J. S., Duplissy, J., Adamov, A., Almeida, J., Bernhammer, A.-K., Breitenlechner, M., Brilke, S., Dias, A., Ehrhart, S., Flagan, R. C., Franchin, A., Fuchs, C., Guida, R., Gysel, M., Hansel, A., Hoyle, C. R., Jokinen, T., Junninen, H., Kangasluoma, J., Keskinen, H., Kim, J., Krapf, M., Kürten, A., Laaksonen, A., Lawler, M.,Leiminger, M., Mathot, S., Möhler, O., Nieminen, T., Onnela, A., Petäjä, T., Piel, F. – M., Miettinen, P., Rissanen, M. P., Rondo, L., Sarnela, N., Schobesberger, S., Sengupta, K., Sipilä, M., Smith, J. N., Steiner, G., Tomè, A., Virtanen, A., Wagner, A.C., Weingartner, E., Wimmer, D., Winkler, P. M., Ye, P., Carslaw, K. S., Curtius, J., Dommen, J., Kirkby, J., Kulmala, M., Riipinen, I., Worsnop, D.R., Donahue, N. M. and Baltensperger, U., The role of low-volatility organic compounds in initial particle growth in the atmosphere, Nature, 533, 527-531, 2016, doi:10.1038/nature18271.

Vanhanen, J., Mikkilä, J., Lehtipalo, K., Sipilä, M., Manninen, H. E., Siivola, E., Petäjä, T., and Kulmala, M.: Particle size magnifier for nano-CN detection. Aerosol Sci. Technol., 45:533–542, 2011.

Suni, T., Kulmala, M., Hirsikko, A., Bergman, T., Laakso, L., Aalto, P. P., Leuning, R., Cleugh, H., Zegelin, S., Hughes, D., van Gorsel, E., Kitchen, M., Vana, M., Hõrrak, U., Mirme, S., Mirme, A., Sevanto, S., Twining, J., and Tadros, C.: Formation and characteristics of ions and charged aerosol particles in a native Australian Eucalypt forest, Atmos. Chem. Phys., 8, 129-139, 2008, doi:10.5194/acp-8-129-2008.

Svenningsson, B., Arneth, A., Hayward, S., Holst, T., Massling, A., Swietlicki, E., Hirsikko, A., Junninen, H., Riipinen, I., Vana, M., Dal Maso, M., Hussein, T., and Kulmala, M.: Aerosol particle formation events and analysis of high growth rates observed above a subarctic wetland-forest mosaic, TellusB, 60B, 353–364, 2008.

Vana, M., Kulmala, M., Dal Maso, M. and Hõrrak, U., Comparative study of nucleation mode aerosol particles and intermediate air ions formation events at three sites, J. Geophys. Res., VOL. 109, D17201, 2004, doi:10.1029/2003JD004413.

Vana, M., Ehn, M., Petäjä, T., Vuollekoski, H., Aalto, P., de Leeuw, G., Ceburnis, D., O'Dowd, C. D., and Kulmala, M. Characteristic features of air ions at Mace Head on the west coast of Ireland, Atmos. Res., 90, 278-286, 2008, DOI: 10.1016/j.atmosres.2008.04.007.

Vanhanen, J., Mikkilä, J., Lehtipalo, K., Sipilä, M., Manninen, H. E., Siivola, E., Petäjä, T. and Kulmala, M. (2011), Particle Size Magnifier for Nano-CN Detection, Aerosol Sci. Technol., 45: 4, 533 — 542, 2011, DOI: 10.1080/02786826.2010.547889.

Wagner, R., Manninen, H. E., Franchin, A., Lehtipalo, K., Mirme, S., Steiner, G., Petäjä, T., and Kulmala, M.: On the accuracy of ion measurements using a Neutral cluster and Air Ion Spectrometer, Bor. Environ. Res., 21, 230-241, 2016.

Wang, J., Krejci, R., Giangrande, S., Kuang, C., Barbosa, H. M. J., Brito, J., Carbone, S., Chi, X., Comstock, J., Ditas, F., Lavric, J., Manninen, H. E., Mei, F., Moran-Zuloaga, D., Pöhlker, C., Pöhlker, M. L., Saturno, J., Schmid, B., Souza, R. A. F., Springston, S. R., Tomlinson, J. M., Toto, T., Walter, D., Wimmer, D., Smith, J. N., Kulmala, M., Machado, L.A. T., Artaxo, P., Andreae, M. O., Petäjä, T., and Martin, S. T., Amazon boundary layer aerosol concentration sustained by vertical transport during rainfall, Nature, 2016, doi:10.1038/nature19819.

Wang, M., and Penner, J. E., Aerosol indirect forcing in a global model with particle nucleation, Atmos. Chem. Phys., 9:1, 239-260, 2009.

Yu, F., and Luo, G.' Simulation of particle size distribution with a global aerosol model: contribution of nucleation to aerosol and CCN number concentrations, Atmos. Chem. Phys., 9: 20, 7691-7710, 2009.

Zhou, J., Swietlicki, E., Hansson, H. C. and Artaxo, P.: Submicrometer aerosol particle size distribution and hygroscopic growth measured in the Amazon rain forest during the wet season, J. Geophys. Res. D Atmos., 107(20), doi:10.1029/2000JD000203, 2002.

Tables

Table 1. Overall data availability for the measurements presented in the manuscript.

		# of days with rain data	# of days with rain event	NAIS particle data	NAIS ion data	NPF
2011	August	5	2	0	0	0
	September	6	1	4	4	0
	October	28	14	31	31	0
	November	30	18	30	30	0
	December	31	23	16	16	0
total 2011		**100**	**58**	**81**	**81**	**0**
2012	January	31	31	31	31	0
	February	29	18	29	29	0
	March	31	0	9	9	0
	April	30	29	29	29	0
	May	31	25	16	16	0
	June	30	23	4	4	0
	July	31	24	0	0	0
	August	31	12	0	0	0
	September	30	4	0	0	0
	October	31	0	0	0	0
	November	30	5	0	0	0
	December	31	24	16	16	0
total 2012		**366**	**195**	**134**	**134**	**0**
2013	January	31	26	31	31	0
	February	28	28	28	28	0
	March	31	24	31	31	0
	April	30	29	30	30	0
	May	31	27	31	31	0
	June	30	23	30	30	0
	July	31	9	31	31	0
	August	31	15	26	26	0
	September	30	13	30	30	0
	October	30	16	31	31	0
	November	30	24	30	30	0
	December	31	17	31	31	0
total 2013		**364**	**251**	**360**	**360**	**0**
2014	January T0t (rain data only from T0t)	20	13	25	25	0
	January T3	0	0	5	5	2
	February	28	23	28	28	2
	March	31	28	31	31	4
	April	30	27	23	23	0
	May	0	0	0	0	0
	June	0	0	0	0	0
	July	0	0	0	0	0

		# of days with rain data	# of days with rain event	NAIS particle data	NAIS ion data	NPF
	August	31	13	6	6	0
	September	30	16	30	12	0
	October	31	19	13	13	0
total 2014		**201**	**139**	**161**	**143**	**8**
total		**1031**	**643**	**736**	**718**	**8**

Table 2. A comparison of the two measurement sites and the wet and the dry season. The values from the pasture site are on the left-hand side, the values from the inside the rainforest site on the right- hand side. The months for the wet season are January to June and July to December for both measurement sites. Aerosol and ion parameters from the NAIS measurements listed are: the ion concentrations in three size bins (0.8-2, 2 - 4 and 4 - 12 nm); the neutral particle concentrations in two different size bins from the NAIS (2 - 4 and 4 -12 nm), and the total particle concentrations (>10 nm) from the MAO CPC measurements and the calculated condensation sink values from the SMPS are also shown. The numbers present median values and the 25^{th}-75^{th} percentiles are in the brackets. The environmental parameters shown are the temperature, the relative humidity, the precipitation rate, the wind direction and the wind speed.

	Pasture site (T3)		Inside rainforest (T0t)	
Particle and ion concentrations				
Season	*Wet*	*Dry*	*Wet*	*Dry*
Cluster ions (0.8-2 nm) [cm^{-3}]	1300(-) (1000-1800)	890(-) (468-1400)	856 (-) (535 -1300) 549(+) (298 - 924)	952(-) (637-1400) 537 (+) (297-915)
Intermediate ions (2-4 nm) [cm^{-3}]	6 (-) (4-11)	5(-) (1-10)	17(-) (10-28) 34(+) (20-48)	17 (-) (10-28) 34(+) (21-48)
Large ions (4-12 nm) [cm^{-3}]	20(-) (11-32)	12(-) (4 - 25)	8(-) (4-16) 8(+) (4-14)	8(-) (4-16) 8 (4-14)
Intermediate particles (2-4 nm) [cm^{-3}]	612 (304 - 1000)	640 (291 - 1200)	358 (128-713)	404 (155-819)
Large particles (4 - 12 nm) [cm^{-3}]	363 (196 - 675)	314 (179 - 551)	115 (42-250)	141(-) (52-313)
CPC total particles (>10 nm) [cm^{-3}]	928 (516 - 1500)	2000 (1100 - 3000)	-	-
SMPS condensation sink [s^{-1}]	$1.9x10^{-3}$ ($9.5x10^{-4}$-$2.4x10^{-3}$)	$5.2x10^{-3}$ ($2.3x10^{-3}$-$6.1x10^{-3}$)	-	-
Environmental parameters				
Temp [°C]	26 (24.4 – 29.9)	25.9 (24.5 – 28.6)	24.1 (23.2 -25.6)	24.5 (23.4 - 26.5)
RH [%]	92.8 (76 – 97.3)	94.6 (83 - 98)	96.9 (93-98)	94.4 (87 - 97)
Total average precipitation [mm]	35.6	49	578	236
Wind direction [°; relative to north]	114.7 (32.7 – 231.5)	94.7 (45.8 – 178.6)	94 (58-138)	105 (58 - 167)
Wind speed [m s^{-1}]	1.1 (0.5 – 2.1)	1.3 (0.6 – 2.4)	0.2 (0.2 – 0.3)	0.2 (0.2 – 0.3)

Table 3. The parameters from the pasture site for NPF days and non-event days are shown. The values shown are: the median total particle concentration measured by a CPC, the median neutral particle concentrations measured by the NAIS in two size ranges (2 - 4 and 4 - 12 nm), and the median negative ion concentrations from the NAIS in three size ranges (0.8-2, 2 - 4 and 4 – 12 nm). The values are calculated for the time window 08:00 – 12:00, which is when the NPF events take place. The numbers in the brackets represent the 25th and 75th percentiles. The second part of the table includes median numbers of environmental parameters for the whole day: temperature, RH, Precipitation and wind direction for NPF /non-event days.

Particle and ion concentrations- 08:00 – 12:00 LT		
	NPF day	**Non NPF day**
Cluster ions (0.8-2 nm) [cm^{-3}]	1000 (-) (862 - 1300)	1000 (-) (865 - 1300)
Intermediate ions (2-4 nm) [cm^{-3}]	10 (-) (5 - 22)	8 (-) (4-15)
Large ions (4-12 nm) [cm^{-3}]	29 (-) (17 - 56)	17 (-) (7 - 33)
Intermediate particles (2-4 nm) [cm^{-3}]	800 (865 - 1300)	640 (281 - 1200)
Large particles (4-12 nm) [cm^{-3}]	785 (446-1300)	321 (170 - 580)
CPC total particles (>10 nm) [cm^{-3}]	1000 (607 - 1900)	938 (400 - 1800)
Full day data		
SMPS Condensation sink [s^{-1}]	1.8x10^{-3} (1x10^{-3}-2.8x10^{-3})	3.2x10^{-3} (1.7x10^{-3}-5.3x10^{-3})
Environmental parameters-full day		
	NPF day	**Non NPF day**
Temp [°C]	26.5 (24.8 – 31.9)	26 (24.4 – 29.2)
RH [%]	90.6 (66.6 –96.3)	93.5 (78.9 – 97.6)
Precipitation rate [mm hr^{-1}]	0.16 (0.15 – 0.35)	0 (0 – 0.16)
Wind direction [°; relative to north]	83.8 (7.3 – 200.6)	104.2 (39.6 – 215.5)
Wind speed [m s^{-1}]	0.9 (0.23 – 1.8)	1.25 (0.6 – 2.3)

Table 4. The growth rates (GR, nmh^{-1}) and the nucleation rates (J; $cm^{-3}s^{-1}$) determined from the NAIS ion and particle data for each nucleation event are presented. Both, the GR values and the nucleation rates present median values for positive and negative ions. Also, the median values for the calculated condensation sink values (CS; s^{-1}) for each event are shown. The condensation sink parameter is calculated from the SMPS size distributions. The last line of the table shows the median values for GR and J for all the nucleation event days are shown, except the ion GR at 2-3 nm of 19.8 nmh^{-1} on 06.02.2014 is considered to be an outlier and not included in the median.

Size bins	**2-3 nm**				**3-7 nm**				
	Particles		*ions*		*Particles*		*Ions*		
	GR (nm h^{-1})	**J** ($cm^{-3}s^{-1}$)	**GR** (nm h^{-1})	**J** ($cm^{-3}s^{-1}$)	**GR** (nm h^{-1})	**J** ($cm^{-3}s^{-1}$)	**GR** (nm h^{-1})	**J** ($cm^{-3}s^{-1}$)	**CS** (s^{-1})
29.01.2014	0.8	0.19	1.4	0.003	2.8	0.097	1.7	0.001	-
30.01.2014	-	-	3.7	0.011	13.6	-	7.1	0.13	0.00076
06.02.2014	0.8	-	19.8	0.07	29	0.87	11	0.01	0.0016
12.02.2014	0.7	0.17	1.2	0.005	1.3	0.09	1.2	0.003	0.0016
12.03.2014	1.1	0.2	1.7	0.002	13.3	-	11.2	0.008	0.0014
13.03.2014	1.5	0.2	1.6	-	1.2	-	8	-	0.0015
18.03.2014	-	-	0.7	0.002	-	-	7.7	0.009	0.0017
25.03.2014	0.8	0.11	-	-	15.7	0.4	15.8	0.018	0.0017
median	0.8	0.18	1.6	0.004	13.3	0.25	7.85	0.009	0.0016

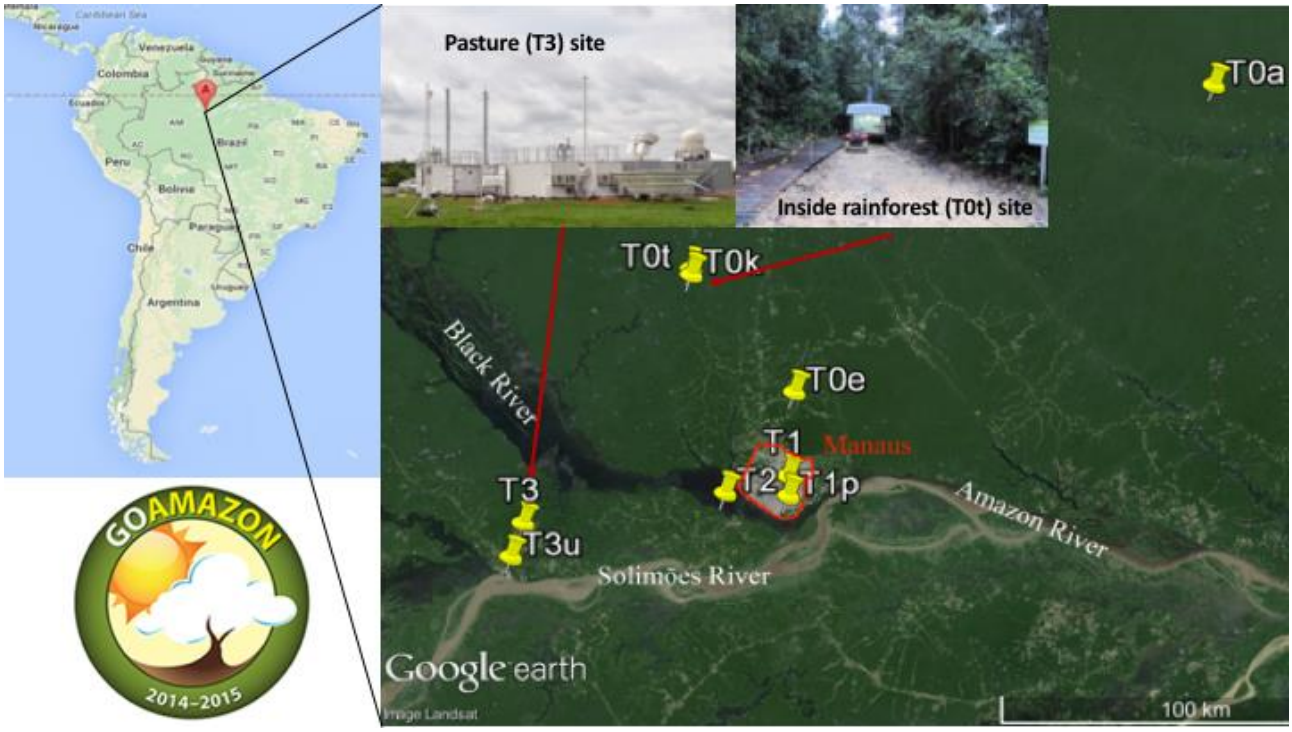

Figure 1. The location on the map and photos of the inside rainforest (T0t) and open pasture (T3) sampling sites in Amazonas is shown here. The left column shows a map of South America and the right-hand side shows a satellite view and photos of the T0t and T3 environment.

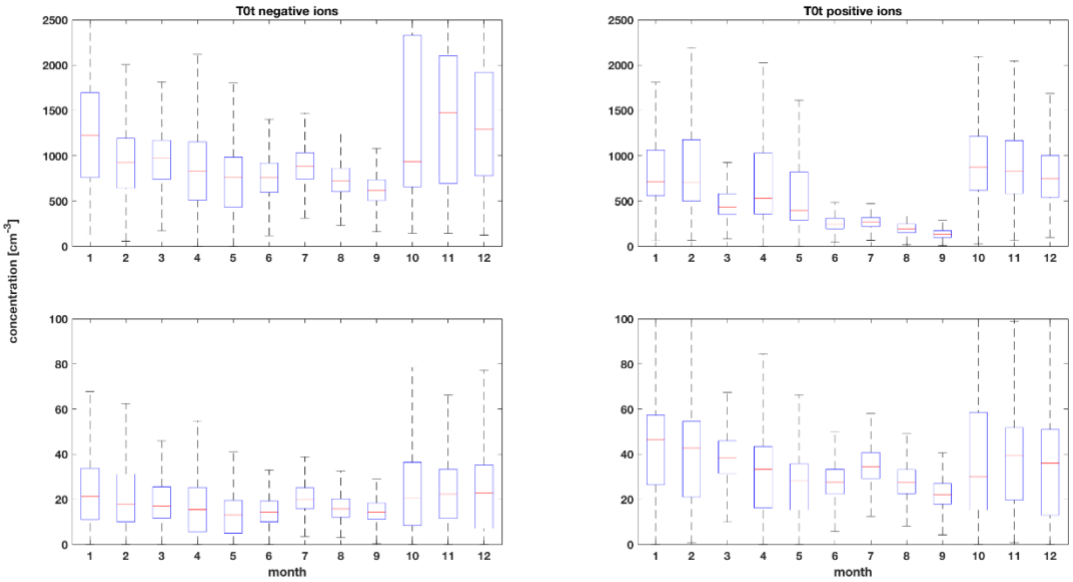

Figure 2. The median annual variations for positive and negative cluster (0.8 – 2nm) and intermediate (2 - 4 nm) ions, from the inside the rainforest site are shown. The boxes show the 25th-75th percentile and the whiskers are 1.5 x IQR (interquartile range), data points beyond the whiskers are considered outliers.

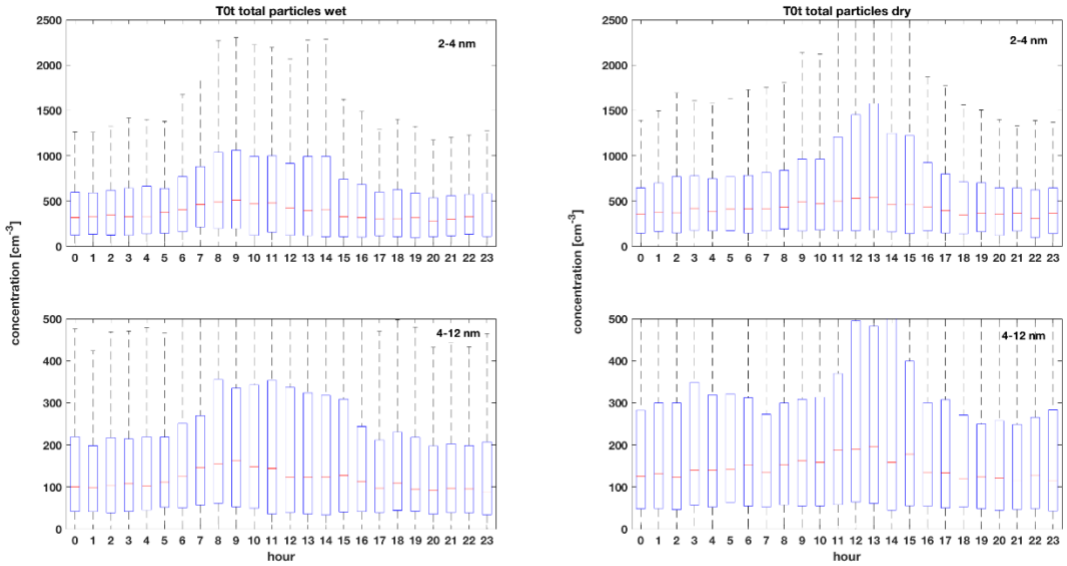

Figure 3. The median diel patterns of the intermediate (2-4 nm) and the large (4-12 nm) particles from the NAIS measurements at the T0t measurement site are shown. On the left -hand side are the values for the wet and on the right-hand side the values for the dry season. The boxes represent 25^{th} – 75^{th} percentiles and the whiskers are 1.5 x IQR (interquartile range), data points beyond the whiskers are considered outliers.

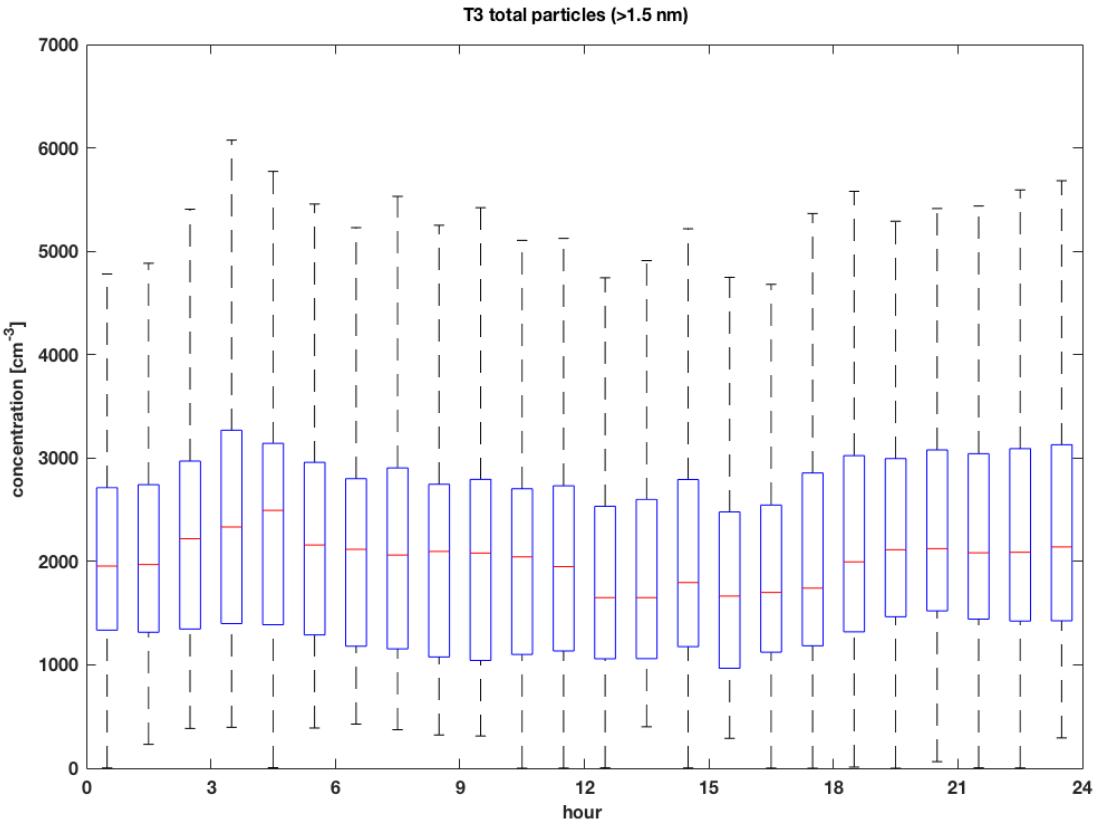

Figure 4. The diel cycle of particles bigger than 1.5 nm measured by the PSM during the dry season at the pasture site is shown. In total, 38 days of data were used. The data show hourly median concentrations, the boxes represent the 25th and 75th percentiles and the whiskers are 1.5 x IQR (interquartile range), data points beyond the whiskers are considered outliers.

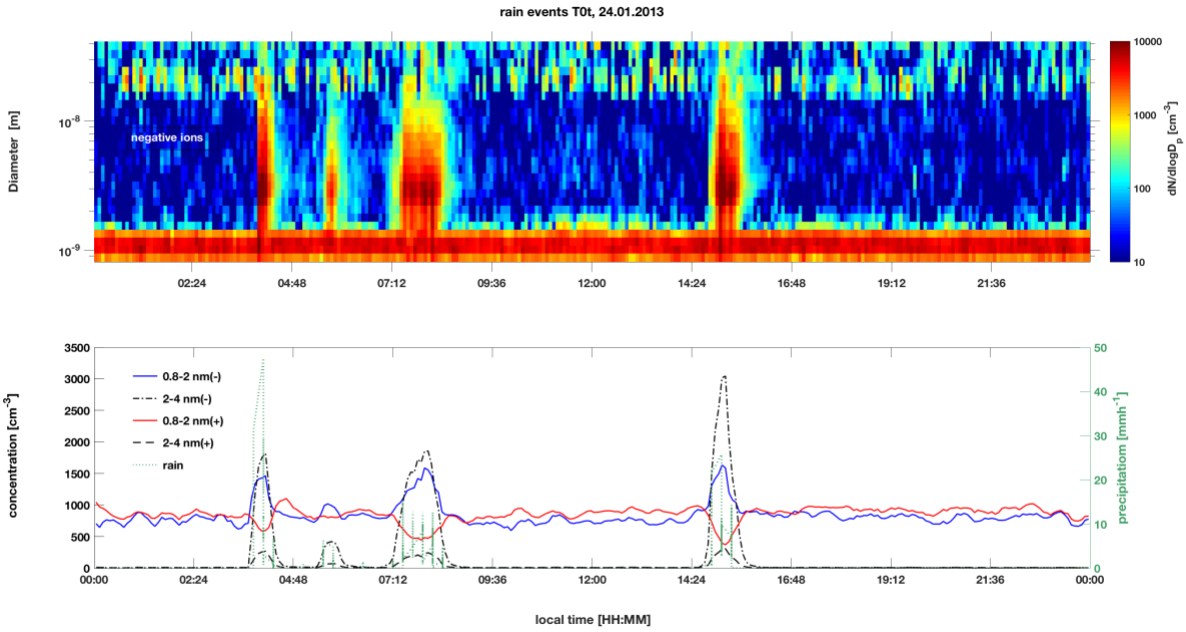

Figure 5. An example for a rain event at the T0t, inside the rainforest measurement site is shown. The upper panel shows the surface Figure of the NAIS negative ion channel. The lower panel shows (i) the concentrations of positive (red line), (ii) negative (blue line) cluster ions (0.8 – 2 nm), (iv) positive (dashed black line), and (v) negative (dot-dashed line) intermediate (2 -4 nm) ions on the left - hand axis. The precipitation rate in mmh^{-1} is shown in green on the right - hand axis.

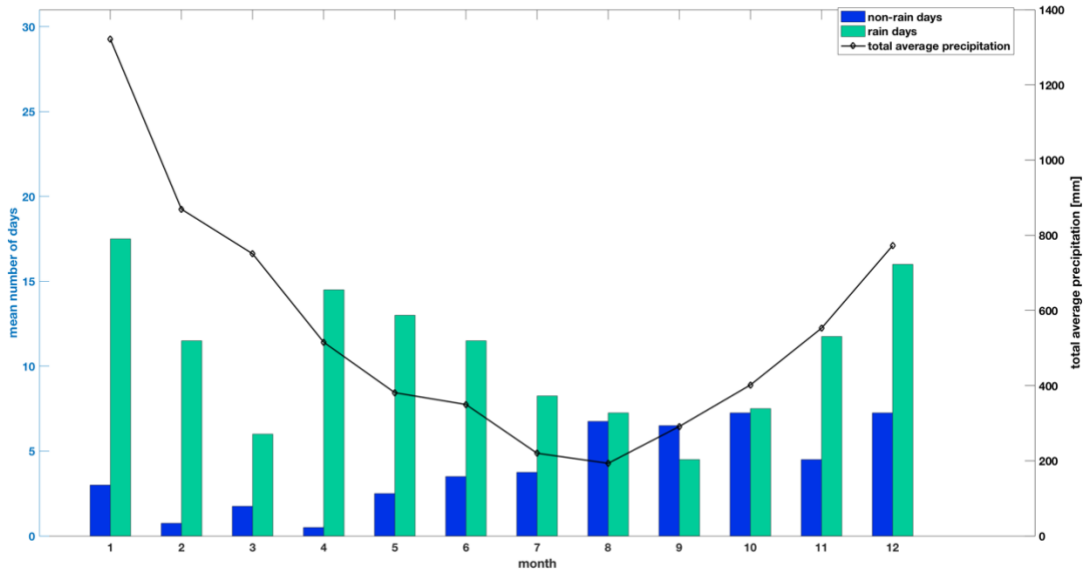

Figure 6. The statistics of the precipitation days at the T0t site are shown. The blue bars show the mean number of days per month with no precipitation and the green bars the mean number of days per month with precipitation rates above zero. The black line shows the average total precipitation per month in mm on the right-hand axis.

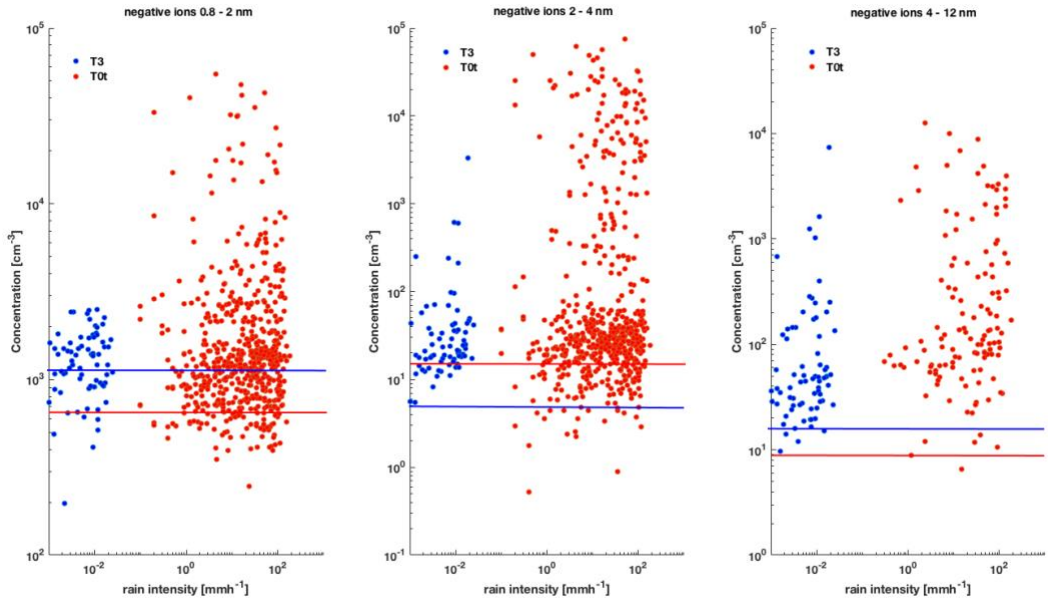

Figure 7. The maximum (99 percentile) negative ion concentrations as a function of rain intensity at the inside rainforest site (T0t) between September 2011 and January 2014 (red circles) are shown. For comparison, the ion concentrations from the open pasture site are added (blue circles). The lines indicate the median ion concentrations at the absence of precipitation for T0t (red) and T3 (blue).

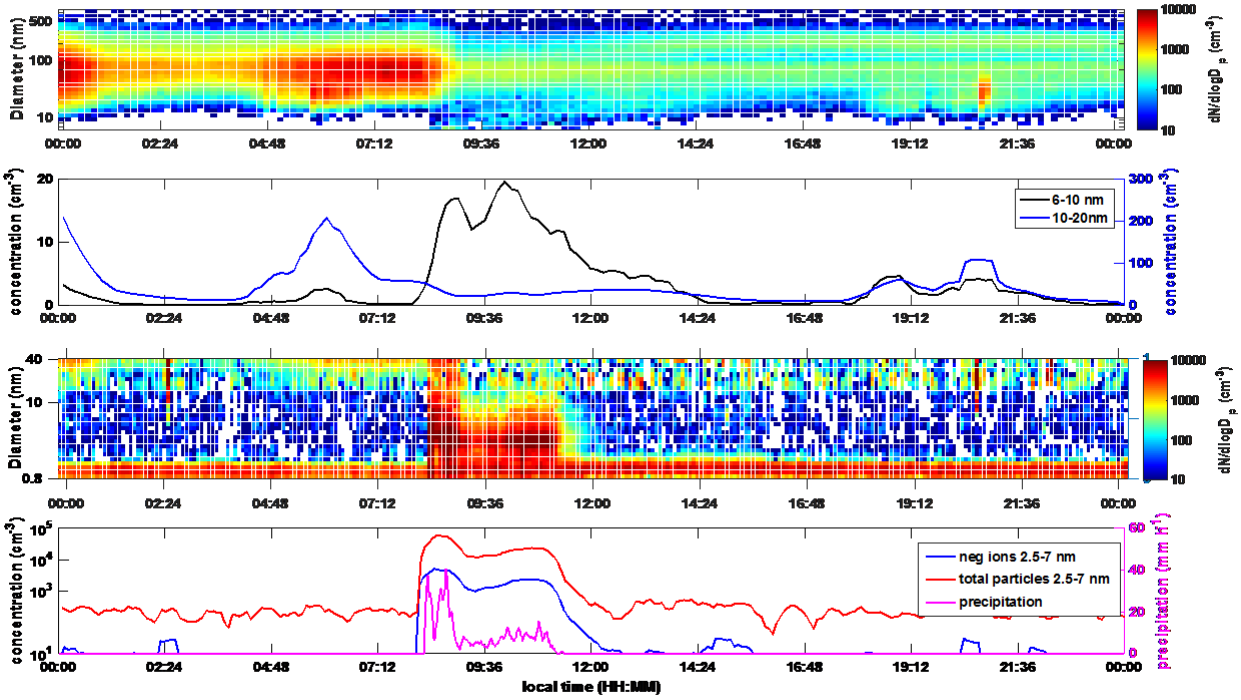

Figure 8. An Example for of a rain-induced event is shown. The upper panel shows the surface Figure for total particles (DMPS). The second panel from the top shows the particle concentrations measured by the DMPS for the size range of 6-10 nm (black line, left-hand axis) and the size range of 10-20 nm (blue line, right-hand axis). The third panel from the top shows the surface Figure for the negative ions, measured by the NAIS. The lower panel shows the negative ion concentrations for 2.5-7 nm in blue and the neutral particle concentration in the same size range from the NAIS in red. For the neutral particles, the scale is on the left-hand axis. The pink trace shows the precipitation rate in mm h^{-1} on the right-hand axis.

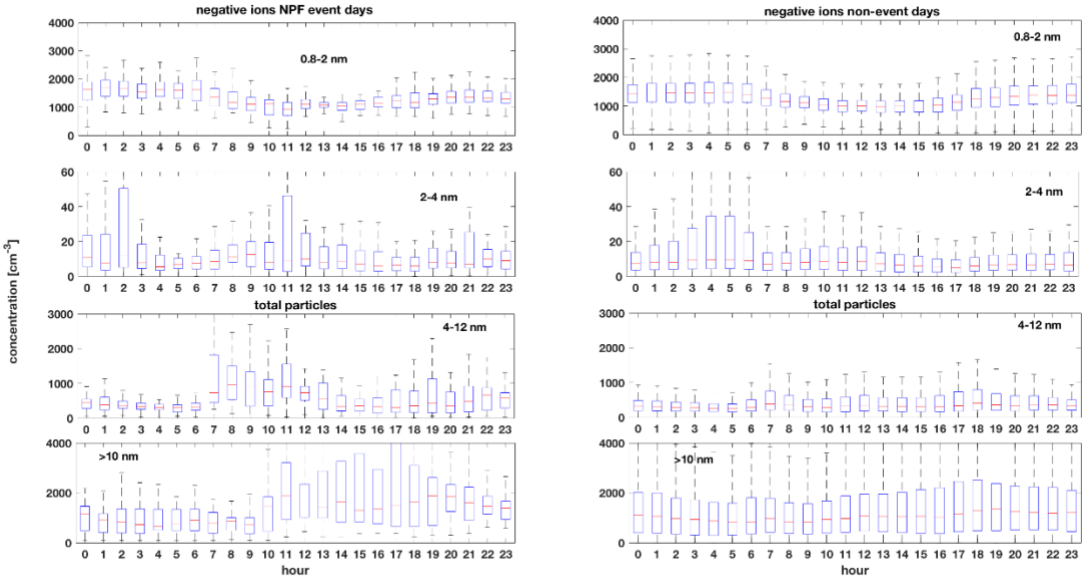

Figure 9. The median diel cycles of cluster ions (0.8 – 2nm), intermediate ions (2 – 4 nm), large (4 – 12 nm) neutral particles, and total particles (>10 nm) for new particle formation event days (left) and non-event days (right) are shown. The boxes show the 25th -75th percentiles and the whiskers are 1.5 x IQR (interquartile range), data points beyond the whiskers are considered outliers.

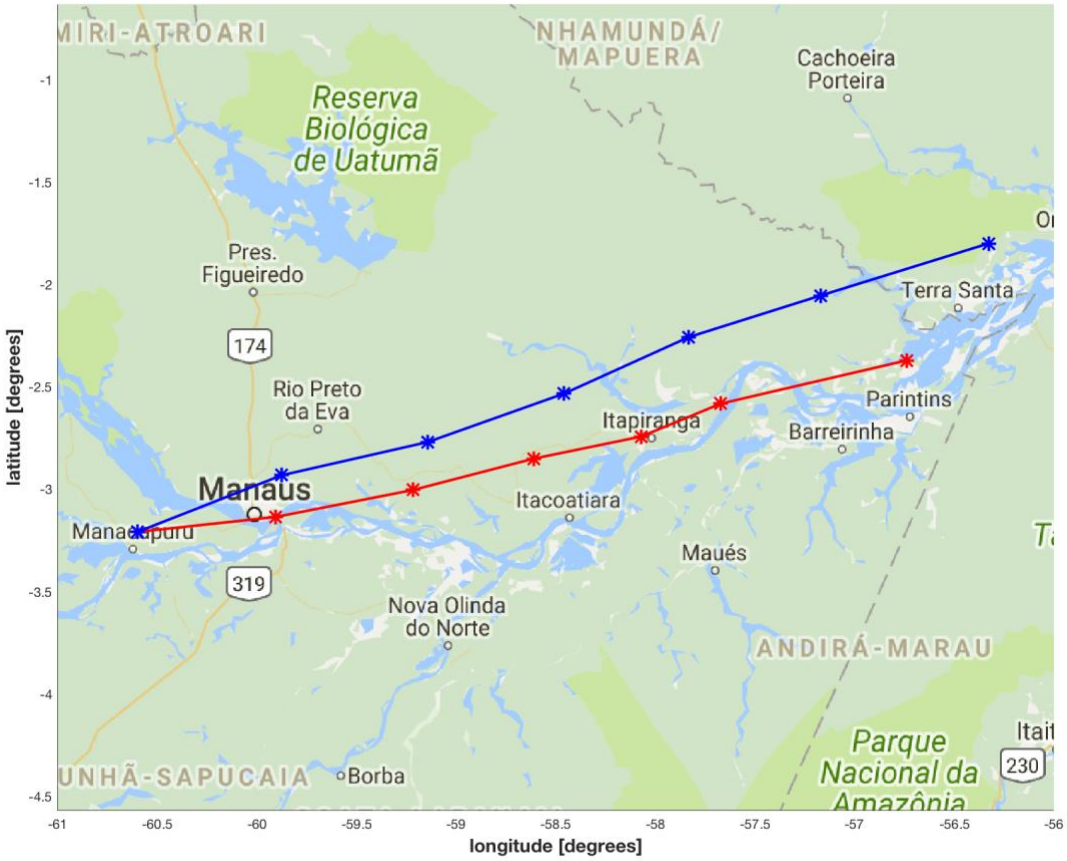

Figure 10. The median back trajectories for NPF (blue) and non-event (red) days are shown. The trajectories were calculated as ensembles, 24hours backwards arriving at 09:00 local time at 500 m a.s.l. at the open pasture measurement site.

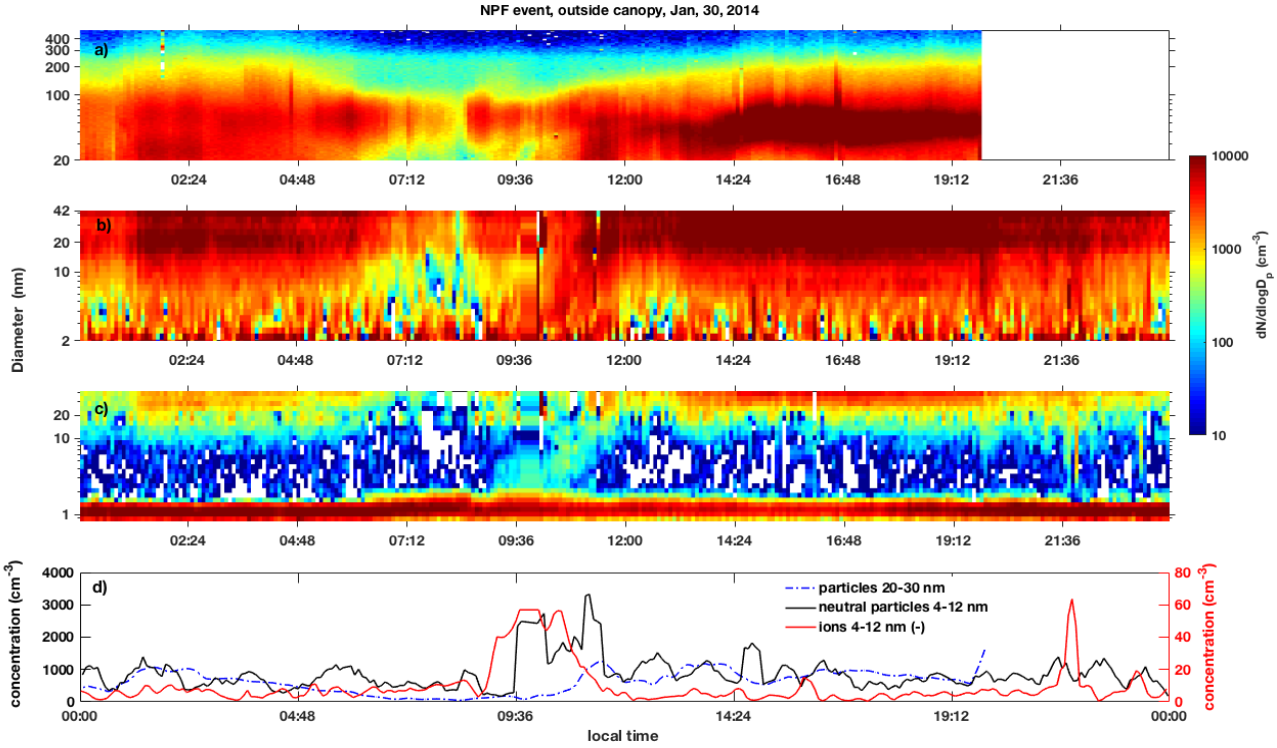

Figure 11. One example of an NPF event day, as observed at the open pasture (T3) site. (a) shows the surface Figure from the SMPS, (b) and (c) show the surface Figures from the NAIS, (b) for neutral particles and (c) for negative ions. The color code indicates the measured concentrations. Panel (d) shows concentrations for the 20-30nm size range from the SMPS on the left-hand axis (blue dashed line). The solid red line shows the 4-12 nm negative ion concentration on the right-hand axis and the solid black line the 4-12 nm neutral particle concentration on the left-hand axis.